UNIVERSIDADE FEDERAL DE SANTA CATARINA
PROGRAMA DE PÓS-GRADUAÇÃO EM CIÊNCIA E ENGENHARIA DE MATERIAIS

César Augusto Stüpp

POWDER METALLURGICAL PROCESSING OF MAGNESIUM-HYDROXYAPATITE COMPOSITES FOR BIOMEDICAL APPLICATIONS

Florianópolis

2015

César Augusto Stüpp

POWDER METALLURGICAL PROCESSING OF MAGNESIUM-HYDROXYAPATITE COMPOSITES FOR BIOMEDICAL APPLICATIONS

Dissertação submetida ao Programa de Pós-Graduação em Ciência e Engenharia de Materiais para a obtenção do Grau de Mestre em Ciência e Engenharia de Materiais.
Orientador: Márcio Celso Fredel
Supervisor/HZG: Norbert Hort

Florianópolis

2015

Ficha de identificação da obra elaborada pelo autor,
através do Programa de Geração Automática da Biblioteca Universitária da UFSC.

Stüpp, César Augusto
Powder Metallurgical Processing of Magnesium-Hydroxyapatite Composites for Biomedical Applications / César Augusto Stüpp ; orientador, Márcio Celso Fredel ; coorientador, Dachamir Hotza. - Florianópolis, SC, 2015.
99 p.

Dissertação (mestrado) - Universidade Federal de Santa Catarina, Centro Tecnológico. Programa de Pós-Graduação em Ciência e Engenharia de Materiais.

Inclui referências

1. Ciência e Engenharia de Materiais. 2. Biomateriais. 3. Magnésio. 4. Hidroxiapatita. 5. Metalurgia do pó. I. Fredel, Márcio Celso. II. Hotza, Dachamir. III. Universidade Federal de Santa Catarina. Programa de Pós-Graduação em Ciência e Engenharia de Materiais. IV. Título.

César Augusto Stüpp

POWDER METALLURGICAL PROCESSING OF MAGNESIUM-HYDROXYAPATITE COMPOSITES FOR BIOMEDICAL APPLICATIONS

Esta Dissertação foi julgada aprovada para a obtenção do título de "Mestre em Ciência e Engenharia de Materiais", e aprovada em sua forma final pelo Programa de Pós-Graduação em Ciência e Engenharia de Materiais.

Florianópolis, 28 de abril de 2015

Prof. Dr. Antônio Pedro Novaes de Oliveira
Coordenador do Programa

Prof. Dr. Márcio Celso Fredel
Orientador

Banca examinadora:

Prof. Dr. Márcio Celso Fredel
Presidente

Prof. Dr. Dachamir Hotza
Coorientador

Prof. Dr. Carlos Augusto Silva de Oliveira

Profa. Dra. Cláudia Ângela Maziero Volpato

Prof. Dr. Jorge Ribeiro Frade

À minha família, seu apoio infindável e às pessoas que foram de extrema importância para realização desse trabalho.

LIST OF FIGURES

LIST OF TABLES

CONTENTS

ACKNOWLEDGEMENTS

First of all, I thank Professor Dr.-Ing. Karl Ulrich Kainer, Director at the Institute of Materials Research and responsible for the operational division "Magnesium Innovation Centre (MagIC)" for providing the opportunity to work at the centre. I thank my supervisor Dr.-Ing. Norbert Hort, Head of the Mg processing department within MagIC in Helmholtz-Zentrum Geesthacht, who is also responsible for this working opportunity. My supervisors in Brazil, Dr.-Ing. Dachamir Hotza and Dr.-Ing Marcio Celso Fredel, who were extremely helpful and mainly responsible for the opportunity in developing this work at Helmholtz-Zentrum. Thank you for all your support before and during the period.

My special thanks are extended to my friends and co-workers Dr. Chamini Mendis, Dr. Marta Mohedano and Mr. Gábor Szakàcs, who helped me in every way, with every single detail of my daily work and doubts I had. Beyond, they are extremely nice and very good friends. The corrosion and coating technology department within MagIC for provision of corrosion testing equipment and Dr. Castern Blawert for giving me access to the laboratories. Mr. Felix Gensch from TU Berlin, who helped us manage everything for hot extrusion. All the materials used were consolidated and extruded at the Research and Development Center for Extrusion at TU Berlin. Dr.-Ing. Frank Feyerabend, who helped and advised me with the immersion tests in biological media.

My office colleagues Mr. Maximilian Hehenberger, Elias Sakkal, Björn Wiese and my department colleagues Dr.-Ing. Juliano Soyama, Mr. Rafael Paiotti, Mr. Ricardo Buzolin and Dr. techn. Domonkos Tolnai, who were responsible for one of the best years I had so far, with their magnificent friendship and trust I will always recall of.

Colleagues and friends who helped me back at my home University with either part of my experimental work or with subjects that required great effort. Mr. Rogério Antônio Campos, Guilherme Wagner, Eduardo Vieira, Pablo Vinícius Souza Lia Fook, André Fook and João Pedro Duarte Tschumi for their friendship, help and time spent together.

My parents, brother and sisters, who encourage my further studies the most, as well as my personal and professional growing. I could have never gotten so far without them.

It is not possible to describe with words how thankful I am for

those all who were friendly, helpful and spent this magnificent time with me. I am everlasting grateful for everything they have done for me.

ABSTRACT

Biodegradable metal alloys are a new class of implant materials suitable for implants such as stents, bone plates and screws. The corrosion of magnesium alloys might provide a new mechanism where they could be used as degradable metal implants to be applied in musculo-skeletal surgery. In this case, a secondary surgery for implant retrieval is not needed. For that, magnesium alloys with controlled *in vivo* corrosion rates need to be developed. There is a high demand to design magnesium alloys with adjustable corrosion rates and suitable mechanical properties. An approach to this challenge is a magnesium metal matrix composite (Mg-MMC) composed of the magnesium alloy ZK60 and hydroxyapatite (HA) particles for tailoring its properties such as mechanical properties and corrosion resistance. The composite was produced by mechanical alloying followed by hot extrusion. HA in contact with molten magnesium releases toxic gases like phosphine (PH_3), so solid-state processing such as mechanical milling and extrusion is feasible. This work presents the influence of different amounts of HA on the degradation behavior and mechanical properties, which shows that the HA addition has a substantial increase in the compression strength (up to 14% for 20 wt.% HA addition) and no negative effect on the controlled degradation behaviour of this biomaterial.

Key-words: magnesium, hydroxyapatite, metal matrix composite, mechanical alloying, biomaterial, powder metallurgy.

RESUMO

Ligas metálicas biodegradáveis são uma nova classe de materiais de implante adequados para a cirurgia óssea. A corrosão de ligas de magnésio pode proporcionar um novo mecanismo onde tais ligas podem ser utilizadas como implantes metálicos degradáveis a serem aplicados em cirurgia músculo-esquelética. Nestes casos, a segunda cirurgia para retirada do implante não seria necessária. Para isso, ligas de magnésio com taxas de corrosão *in vivo* controladas precisam ser desenvolvidas. Há uma grande procura para projetar ligas de magnésio com taxas de corrosão ajustáveis e propriedades mecânicas aplicáveis. Uma abordagem a este desafio é um compósito de matriz metálica (CMM) composto pela liga de magnésio ZK60 e hidroxiapatita (HA) para aperfeiçoar suas propriedades como resistência mecânica e resistência à corrosão. O compósito é produzido via moagem de alta energia seguida de extrusão à quente. Uma vez que HA em contato com magnésio líquido libera gases tóxicos como fosfina (PH_3), esta é a melhor forma de sua produção. Este trabalho mostra a influência de diferentes quantidades de hidroxiapatita na taxa de degradação e propriedades mecânicas do compósito, as quais evidenciam um aumento substancial na resistência à compressão com a adição de HA (até 14% para o compósito com 20% de HA), sem detrimento às propriedades de degradação controlada do biomaterial.

Palavras-chave: magnésio, hidroxiapatita, compósito de matriz metálica, moagem de alta energia, biomaterial, metalurgia do pó.

1 INTRODUCTION

Research in Mg has grown substantially in the last decades increasing the types of applications that use Mg. Mg has a high specific strength (strength-to-density ratio - σ/ρ) (CZERWINSKI et al., 2011), owing the low density of these alloys. Advantages of magnesium alloys as biomaterials resulted in growth of this field in the last two decades (KIRKLAND; BIRBILIS, 2013).

Non-toxicity, degradability, biocompatibility and mechanical properties close to that of bone are reasons of why magnesium is suitable for medical applications (STAIGER et al., 2006; KUHLMANN et al., 2013). Magnesium alloys could fit specially where degradation within a certain amount of time is desired due to their corrosion behavior (KUHLMANN et al., 2013). However, mechanical integrity cannot be compromised by fast corrosion while the healing process is in the embryonic state (NG; WONG; CHENG, 2010).

One of the main advantages of using a reabsorbable implant is a second surgery for its removal is not required (NG; CHIU; CHENG, 2010; KIRKLAND; BIRBILIS, 2013). This excludes possibility of errors during implant's retrieval or revision, in addition to the patient comfort, also saves money and time (KIRKLAND; BIRBILIS, 2013). The main advantage of using a biodegradable implant is that it is likely to return the affected joint very close to its original condition (YUN et al., 2009). In case of magnesium alloys, corrosion products can be metabolized within a period of time (SONG, 2007). Magnesium is a common constituent in the human body, where at least half of the magnesium is stored in bone tissues (NG; CHIU; CHENG, 2010).

Rapid corrosion can result in loss of mechanical integrity before the surrounded tissue has enough time to heal (WITTE et al., 2006). One approach for solving the fast corrosion rate is the development of a metal matrix composite (MMC), where ceramic particles are distributed within the magnesium matrix (WITTE et al., 2007; LI, 2010; FENG; HAN, 2010; HE et al., 2011). This work describes a specific processing route to manufacture a composite composed of magnesium alloy as the matrix and hydroxyapatite (HA) particles as the reinforcement. The degradation behavior in biological media, mechanical properties and their effect on amount of HA are investigated.

The main aim is to understand the effect of changing the volume fraction of HA in ZK60 alloy on the resultant microstructure, the degradation in biological media and on the corrosion products.

2 MOTIVATION AND RESEARCH OBJECTIVES

Due to the increased demand for orthopedic implants, new alternatives for materials that satisfy the mechanical and degradation properties are sought. The mechanical properties, corrosion resistance and biocompatibility are extremely important for a good correlation between body and implant.

A biodegradable material means a second surgery is not needed thus removing any possible problems related to its retrieval. A biomaterial that has properties very close to that of bone and whose degradation products are beneficial to physiological system is an appreciable advance in the use of degradable implants.

With that in mind, a composite with magnesium as base material was developed. Hydroxyapatite particles are added for tailoring its properties, specially the biodegradation of the composite. The composite was produced via mechanical alloying, followed by hot extrusion, from which specimens are fabricated and tested. Four composites with different amounts of hydroxyapatite were studied: 7.5 wt.%, 10 wt.%, 20 wt.% and 0 wt.% for comparison. In this thesis, the composite additions are shown in wt.%[1]. In volume percentage, the additions 7.5 wt.%, 10 wt.% and 20 wt.% would be 5 vol.%[2], 6 vol.% and 13 vol.% respectively.

The specific objectives are as follows:

1. Achieve a uniform distribution of hydroxyapatite particles in magnesium matrix after mechanical alloying and also after hot extrusion.

2. By selecting different quantities of hydroxyapatite, achieve controlled corrosion rates.

3. Reach composite's mechanical properties to that of bone.

[1] wt.% is an abbreviation for weight percentage.
[2] vol.% is an abbreviation for volume percentage.

3 STATE OF THE ART

3.1 BIOMATERIALS

The *European Society for Biomaterials Consensus Conference II* defines biomaterials as "materials intended to interface with biological systems to evaluate, treat, augment, or replace any tissue, organ, or function of the body". They should be biocompatible, which means the ability of a material to interact with its host without triggering an adverse immune response (identification of a foreign material by white blood cells followed by their effort to destroy it) and fulfill its functions without harming the patient. (NEWELL, 2009)

In orthopedic medicine, implants are normally used for correcting loss of function of the skeletal system due to a deformity or an accident. There are different devices for each kind of situation, including screws, joints (hip, knee, elbow, shoulder) and bone plates. (MUDALI; SRIDHAR; RAJ, 2003)

When it comes to degradable biomaterials, the most important feature is a link between slow uniform corrosion and the retention of mechanical properties degradation (ZHANG et al., 2012).

A biodegradable material used in orthopedic surgery must be completely functional before and during healing of surrounding tissue (SONG, 2007). The implant should support imposed loads, until the bone has enough strength to function. After healing, degradation rate cannot exceed an acceptable rate, otherwise degradation products will be released too fast and the body will not be able to metabolize the degradation products (SONG, 2007). One important advantage of biodegradable materials is that they are likely to return the injured tissue closer to its original condition (YUN et al., 2009).

The ideal implant would behave as illustrated in Figure 1. While bone gradually recovers, the material keeps its mechanical integrity. After the bone heals to a certain point (green area), implant's degradation can start without overloading the bone which is not yet completely healed.

Biomaterials are made from ceramics, metals, polymers and their composites. Each group has their advantages and disadvantages in envisaged applications.

Ceramics are inorganic compounds and chemically stable within the body, e.g. alumina, zirconia, bioactive glass and calcium phosphate (MUDALI; SRIDHAR; RAJ, 2003). The disadvantages are: low tensile

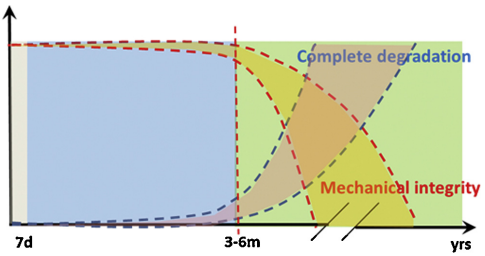

Figure 1 – *Ideal behaviour of biodegradable implant material in agreement with bone's recovering process (figure adapted from (ZHENG; GU; WITTE, 2014)).*

strength and fracture toughness and susceptibility to fracture when overloaded (MUDALI; SRIDHAR; RAJ, 2003). The most well known ceramic biomaterials are alumina, zirconia and hydroxyapatite, as they are normally biocompatible and bioinert while some ceramics can be bioactive, have high compressive strength and are visible, as dental implants.

Polymers undergo relatively fast corrosion in physiological environments and are used as degradable implants. The breakdown of polymers cause decrease in mechanical properties as well as tissue irritation (MUDALI; SRIDHAR; RAJ, 2003). Many polymers are used as biodegradable materials. However, their mechanical properties are less than those of their competitors, specially during degradation. One example of a polymer as biomaterial is Nylon, which has the advantage of low cost and good processability, but degrades and deforms over time (KIRKLAND; BIRBILIS, 2013). PLA (polylactic acid) is another example of degradable biopolymer, presenting renewability, biodegradability, biocompatability and good thermomechanical properties. (RAQUEZ et al., 2013)

Metals have a combination of relatively high Young's modulus and yield strength with ductility, making them suitable for load-bearing applications, without permanent dimensional changes and large deformations (MUDALI; SRIDHAR; RAJ, 2003). Metals are well known for their ability to bear significant loads, adequate fatigue catastrophic properties and for the substantial amount of plastic deformation (AGRAWAL, 1998). On the other hand, some disadvantages include stress shielding in long term implants (in the case of an ortophedical implant, the load

is shared between bone and implant. The load imposed to both will be a function of their Young's modulus. When implant's modulus is much higher than that of bone, the latter will bear a significantly lower load, weakening it. (AGRAWAL, 1998)) and the release of toxic ions in alloys which are not corrosion resistant (UHTHOFF; POITRAS; BACKMAN, 2006; WITTE et al., 2008). The commonly used metals for biomedical applications are stainless steel and titanium (AGRAWAL, 1998; MUDALI; SRIDHAR; RAJ, 2003). Some examples are hip joints, screws and other parts used for bone fixation (KIRKLAND; BIRBILIS, 2013).

Composites are a combination of two or more of the materials described above. They are usually composed of two components: the matrix and the reinforcement, while the latter tailors the properties of the matrix. The inherent weaknesses of metals, ceramics and polymers limits their applications in biological settings. This can be overcome by choosing a composite that could enhance the desired properties of each of the components. Examples of this are ceramic reinforced metallic materials where strength of the metal is enhanced by adding a second phase.

3.2 MAGNESIUM ALLOYS

The Young's modulus of Mg is very close to that of bone (around 45 GPa (WWW.MATWEB.COM, 2014)), they have high specific strength and are biodegradable. Nevertheless, the fast degradation is a problem because it compromises the mechanical properties while load bearing is still needed. The body has to metabolize the quickly released corrosion products of Mg alloys. This problem is normally overcome by different methods as coating, alloying and magnesium based composites.

Magnesium can be alloyed with many different elements. The alloying additions are used to improve or achieve needed design properties for the envisaged applications. For magnesium, aluminum is the most used element for alloying. Since 1920's, mechanical and corrosion properties of Mg-Al alloys are already established (KAINER, 2003). Magnesium is also alloyed with several other elements. Some examples are calcium, manganese, rare earth elements, silicon, zinc and zirconium, each having one or more specific effects on the final alloy (KAINER, 2003). Each alloy has a denomination standardized by ASTM, which are two letters indicating the main alloying elements followed by their respective nominal weight in percentage (KAINER, 2003). Table 1 shows some examples of element designation in magnesium alloys.

Table 1 – ASTM designations for some of magnesium alloying elements. (KAINER, 2003)

Abbreviation letter	Alloying element
A	Aluminum
B	Bismuth
X	Calcium
M	Manganese
S	Silicon
Z	Zinc
K	Zirconium

3.2.1 Mechanical behaviour of magnesium

The crystal structure has an important role on mechanical properties. In magnesium, the crystal lattice is built by two repetitious layers of atoms (B and A), forming a hexagonal closed-packed (hcp) structure, illustrated in Figure 2. (HAYDEN; MOFFATT; WULFF, 1965) The c/a ratio of Mg is 1.625 with lattice parameters c=0.52 nm and a=0.32 nm. The c/a ratio in hexagonal metals determines the activation of deformation mechanisms, as crystallographic slip and twinning, explained hereafter. (KAMMER, 1998; AL-SAMMAN, 2008)

Metallic materials normally deform by crystallographic slip. For metallic materials to deform plastically by crystallographic slip, at least five independent slip systems are needed described by the Von Mises criterion. Due to the hexagonal structure of magnesium, it has less than five independent slip system at room temperature and deform essentially by basal slip and twinning, limiting its deformability (LI et al., 2012). Twinning is one of the most important features in deformation of Mg (BETTLES; GIBSON, 2005).

Due to its low density, magnesium exhibits a high specific strength (strength to density ratio). Figure 3 displays the Young's modulus, yield strength and density of steel, aluminum and magnesium along with their specific properties. As shown, magnesium has lower yield strength and modulus. However, its specific yield strength is higher and its specific modulus is basically the same, compared with other metals such as aluminum alloys and steels.

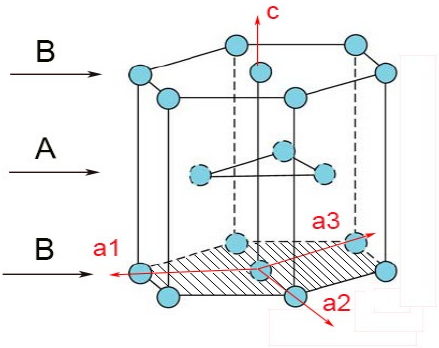

Figure 2 – *Atomic sequence of a hexagonal closed-packed crystal structure and its crystal lattice showing the basal plane. (HAYDEN; MOFFATT; WULFF, 1965)*

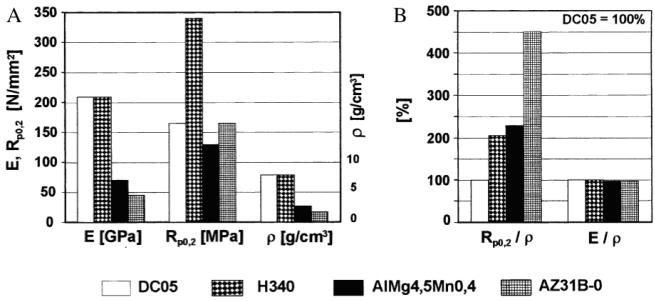

Figure 3 – *Young's modulus (E), yield strength (YS) and density (ρ) of steel, aluminum and magnesium (a) and same showing specific properties (b). (KAINER, 2003)*

3.2.2 Corrosion of magnesium

Corrosion of magnesium is different than in most metals (as iron, steels and copper). Normally, the anodic dissolution rate increases and the cathodic hydrogen-evolution decreases when in acid solution. This is not the case in magnesium which, at first, seems to have the opposite behaviour. (SONG; ATRENS, 2003)

When magnesium gets in contact with water, it immediately sends Mg^{2+} cations into solution, as Equation 3.1 displays (PEKGULERYUZ; KAINER; KAYA, 2013).

$$\text{Anodic reaction} : Mg \rightarrow Mg^{2+} + 2e^{-} \tag{3.1}$$

Concurrently, water dissociation takes place, which is shown by Equation 3.2 (PEKGULERYUZ; KAINER; KAYA, 2013).

$$\text{Dissociation} : H_2O \leftrightarrow OH^{-} + H^{+} \tag{3.2}$$

After Mg^{++} cations are in the solution, remaining electrons stay in the metal, which have to be consumed. Ions H^{+} from water dissociation consume these free electrons, resulting in hydrogen evolution (Equation 3.3). Water dissociation also releases OH^{-} ions into the solution, increasing the pH value. In addition, these ions aid the formation of a passivation layer, shown in Equation 3.4 and in Figure 4. (SONG; ATRENS, 2003; PEKGULERYUZ; KAINER; KAYA, 2013)

$$\text{Cathodic reaction} : 2H^{+} + 2e^{-} \rightarrow H_2 \tag{3.3}$$

$$\text{Product formation} : Mg^{2+} + 2OH^{-} \rightarrow Mg(OH)_2 \tag{3.4}$$

The pH of surrounding medium influences the corrosion behaviour of magnesium, as demonstrated in the Pourbaix diagram (Figure 5). If pH is above 10.5, a self-healing passive layer forms (PEKGULERYUZ; KAINER; KAYA, 2013), although this layer protects the material underneath poorly due to its inherent porosity (SONG; ATRENS, 2003). A partially protective film forms so that general corrosion in magnesium is not the mainly issue, but localized corrosion. Corrosion phenomena are illustrated in Figure 4, where dashed arrows correspond to electron consumption by external polarization and by acidic corrosion. The illustration also shows a $Mg(OH)_2$ layer, which forms as the reactions take place.

The formation of $Mg(OH)_2$ drives the reaction in Equation 3.2 to the right due to disturbance between water and its ions (principle of Le

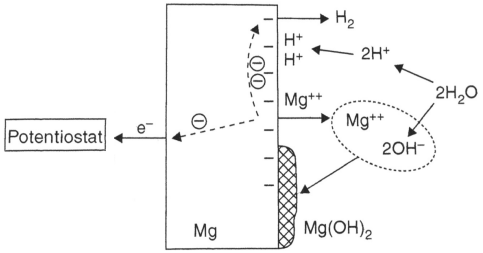

Figure 4 – *Schematic illustration of magnesium corrosion (PEKGULERYUZ; KAINER; KAYA, 2013).*

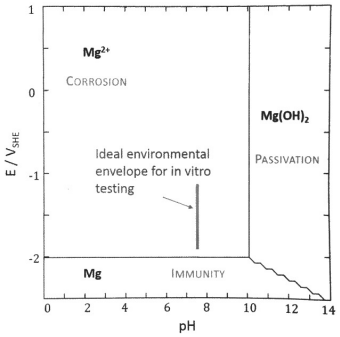

Figure 5 – *Pourbaix diagram for magnesium (KIRKLAND; BIRBILIS, 2013).*

Chatelier and Braun - if a chemical system at equilibrium experiences a change either in concentration, temperature, partial pressure or volume, a new equilibrium is established because the system shifts to neutralize the imposed disturbance). The more ions H^+ are released, more metal is consumed. Summarizing that if magnesium ions are released into the solution, the disassociation of water become more prevalent, increasing the consumption of electrons by hydrogen ions. This results in further dissolution of magnesium and hydrogen evolution. (PEKGULERYUZ; KAINER; KAYA, 2013)

Pourbaix diagram is used to visualize which phase is stable at a given pH and potential, exhibiting areas where different corrosion phenomena occur (KIRKLAND; BIRBILIS, 2013). Pourbaix diagram for

magnesium is shown in Figure 5 displaying the phenomena behind its reactivity.

In magnesium alloys, increasing the pH of the surrounded media will stabilise the corrosion products on the corrosion layer. Therefore, it is an appropriate way of controlling magnesium corrosion (WITTE et al., 2007). One element known to reduce the susceptibility of magnesium to corrosion is calcium, the main constituent of hydroxyapatite (EMLEY, 1996).

Corrosion process in physiological fluids is complicated, as they contain many different substances that make the corrosive medium unique (KIRKLAND; BIRBILIS, 2013). Magnesium corrosion behaviour and the understanding of the corrosion products released within the human body are described in Sections 3.2.5.

3.2.3 Extrusion of magnesium

Magnesium alloys are extruded at elevated temperatures due to avaibility of sufficient deformation modes. Recovery is responsible for material softening above 200°C (KAINER, 2003). Therefore, depending on the alloy, temperatures above 250°C are used for extrusion.

With torsion tests between 180°C and 450°C, Myshlyaev et al. (MYSHLYAEV et al., 2002) showed that at lower temperatures, fracture precedes or shortly follows ultimate tensile strength, Figure 6. Deformation behaviour at higher temperatures is explained by the increasing level of dynamic recovery. This can be related to dislocation climb and activation of additional non-basal slip systems. Dynamic recovery and recrystallization are the major factors that reduce flow stress and raise ductility at high temperatures. (MYSHLYAEV et al., 2002)

Extruded magnesium and its alloys have higher strengths and better corrosion resistance due to grain refinement (ZHANG et al., 2012). This is also true for particle-reinforced magnesium composites, as extrusion promotes a better particle distribution and prevents segregation (WANG et al., 2012).

If the extrusion process is controlled, it can also be used as a grain refining technique. The most influencing parameters, in this case, are working temperature and extrusion ratio, even though effects of the latter are still unclear. (MYSHLYAEV et al., 2002; ZHANG et al., 2012)

Corrosion is controlled not only by chemical composition (LIU et al., 2010), heat treatment (ZHAO et al., 2008) and microstructure (ZENG et al., 2011). Zeng et al. (ZENG et al., 2011) studied the role of extru-

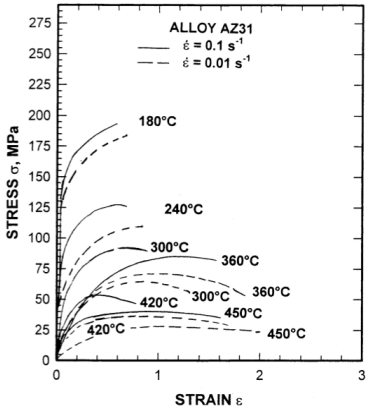

Figure 6 – *True equivalent stress and strain near the surface of AZ31 magnesium alloy shown by representative torsional flow curves. (MYSHLYAEV et al., 2002)*

sion in the corrosion behaviour of ZK60. Zr leads to grain refinement and intermetallic compounds tend to form along the grain boundaries, which for this alloy are MgZn phases. These compounds have a higher potential compared with the magnesium matrix and act as cathodes, therefore, cause pitting corrosion. To illustrate the influence of microstructure, i.e. processing route, in the corrosion rate, Figure 7 illustrates the corrosion behaviour of a conventional polarization test, as function of grain size. (ZENG et al., 2011)

3.2.4 ZK60 magnesium alloy

ZK60 contains nominally 6% zinc, 0.5% zirconium and magnesium is balance (in wt%), with a density of 1.83 g/cm^3.

The biocompatibility of alloying additions is important when choosing alloys for biomedical applications.

Zinc is essential for humans (YAMAGUCHI, 1998). Both zinc and zirconium are corrosion resistant, biocompatible and bioactive (YAMAGUCHI, 1998; LIN et al., 2013). Zinc deficiency causes many physiological functions to be perturbed, such as bone formation, causing metabolic disorders that can be implicated in many diseases (PRASAD; OBERLEAS, 1970; YAMAGUCHI, 1998; FENG; HAN, 2010). Zirconium is

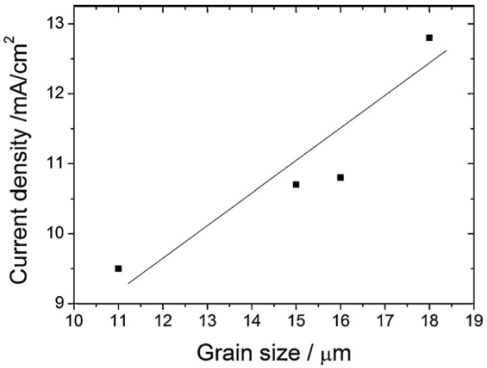

Figure 7 – *Influence of grain size on corrosion rate by conventional polarization tests. (ZENG et al., 2011)*

also found in the human body, but its functions remain unclear (LIN et al., 2013).

ZK60 has been widely studied and its mechanical and corrosion properties are already well established. Therefore, ZK60 seems to be suitable for the development of this work.

3.2.5 Magnesium alloys as biomaterials

As potential biomaterials, magnesium presents benefits and drawbacks and the important conditions of this material follow:

- In former times biomaterials have to be inert in human body, so the body would not see it as a foreign threat. Magnesium itself is known to be biocompatible. In other words, not only magnesium is not harmful to the organisms, but it does not trigger a large immune response. Mg takes part in human body's cycle, helping to increase bone formation rate (HOWLETT et al., 1994).

- Fast degradation rates does not allow metabolization of corrosion products, which can be hazardous. A biocompatible Mg alloy should not release toxic elements. Beyond that, the release rate must be reasonable, even though they are naturally present in the human body (KIRKLAND; BIRBILIS, 2013).

Magnesium is an essential mineral which must be continuously ingested and distributed to cells. Magnesium is processed by intestines, which absorb it as an ion, and kidneys, which excretes its overbalance. As most of magnesium is excreted by kidneys, the recommended daily intake for an adult is around 300 and 420 mg. Apart from its minimum healthy daily intake, an increased magnesium supply can also reduce risks of diseases as osteoporosis and coronary artery disease. (VORMANN, 2003)

Many studies were conducted on the interaction between magnesium and the human body, and show that magnesium is a safe biomaterial. However, release rate of corrosion products must be acceptable for Mg alloys to be used in the body. That means, the living system must be able to metabolize the corrosion products.

During degradation, hydrogen is created as by product (see Section 3.2.2). Hydrogen evolution is not only important for corrosion, but also for health, as hydrogen gas cavities can form (KUHLMANN et al., 2013). Kuhlmann et al. (KUHLMANN et al., 2013) concluded that when implant's degradation is slow enough, H_2 gas is absorbed as fast as it is formed.

Another issue, is that an increase in pH inhibits cell proliferation and tissue formation. A higher pH would form a $Mg(OH)_2$ layer, which attenuates magnesium corrosion. This cannot be used to improve degradation properties, as high pH values are harmful to the viability of cells. If the implant is considered to be a foreign body by the cells, they might migrate or die by apoptosis (programed cell death) or necrosis (cell death by external factor). (YUN et al., 2009)

As discussed, there are a number of properties that make Mg a suitable biodegradable material within the body.

3.3 HYDROXYPATITE IN BIOMEDICAL APPLICATIONS

Hydroxyapatite (HA) possesses low solubility in the human body (FULMER et al., 2002), and it is the main component of the bone. It is widely used in medical applications, due to its biocompatibility and similarity to human bone (MONMATURAPOJ, 2008). Thus, HA can be used as reinforcement in magnesium based composites.

Hydroxyapatite is also a biomimetic material (materials made chemically or physically similar to those produced by living organisms, as an attempt to achieve same properties and sometimes, functions) (NEWELL, 2009) and cannot support mechanical loads due to inherent

brittleness. With a density of 3.10 g/cm^3, it is stable at body pH (KLEIN et al., 1990) and its chemical similarity to bone enables osseointegration (direct contact of HA to bone tissues without the need of a connective membrane, aiding bone formation) (PARK; BRONZINO, 2000). Hydroxyapatite, as a bioactive material, can also aid cell adhesion (YUN et al., 2009).

3.4 MAGNESIUM-BASED METAL MATRIX COMPOSITES

It is very important to combine degradation rate with satisfactory mechanical properties. Normally, when magnesium composites are developed, both corrosion and mechanical properties are studied. The next two Sections address separately these two main topics.

3.4.1 Mechanical properties

In particle reinforced composites, mechanical properties are influenced by the interface between matrix and particles. The mode of strengthening is by load transfer from the ductile matrix to the hard reinforcements. In these composites, the matrix would be reinforced by the high strength of the secondary phases (FENG; HAN, 2010). For that, a good bonding between matrix and reinforcement is necessary, for better load transfer (FENG; HAN, 2010).

Different types of magnesium matrix composites are investigated extensively. Silicon carbide (SiC) reinforced composites is a typical example (WANG et al., 2012; DENG et al., 2012; NIE et al., 2012; SHEN et al., 2013). These composites are developed for improved creep resistance, strength and stiffness (NIE et al., 2012; SHEN et al., 2013). The Young's modulus and tensile strength of these composites are significantly superior to that of the base alloy (SHEN et al., 2013). These properties are achieved with the appropriate ratio of particles, processing route and other intrinsic parameters. For example, the as-cast composites show inferior mechanical properties compared with the as-extruded, because the latter improves particle distribution (WANG et al., 2012; NIE et al., 2012). Furthermore, these particles aid grain refinement, assisting the improve in yield strength and elongation to failure (WANG et al., 2012). However, these composites show extremely high corrosion rates (see Section 3.4.2). This is one of the reasons SiC particles are not recommended for applications where controllable corrosion rates are desired.

Magnesium-alumina (Mg-Al_2O_3) composites have been investigated. In addition to enhanced mechanical properties, Hassan and Gupta (HASSAN; GUPTA, 2006) reported a brittle to ductile behaviour transition and improvement in mechanical properties when nano-sized alumina particles were added. However, as with SiC magnesium composites, the corrosion properties are not improved with alumina (also described in Section 3.4.2). Therefore, they cannot be used in harsh environments.

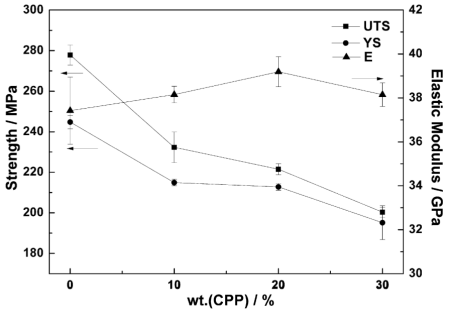

Figure 8 – *Tensile strength, yield strength and Young's modulus for ZK60 magnesium alloy and ZK60/calcium polyphosphate composites with up to 30 wt.% reinforcement. (FENG; HAN, 2010)*

Feng and Han (FENG; HAN, 2010) investigated the behaviour of a calcium polyphosphate (CPP) reinforced ZK60 magnesium composite. A decrease in yield strength and ultimate strength was observed with the addition of up to 30 wt.% CPP. The mechanical properties are shown in Figure 8. They showed that the Young's modulus (E) increases with 0-20 wt.% CPP additions and then decrease. The investigation of the composite with up to 10 wt.% reinforcement illustrate that up to 5 wt.% CPP reinforced composites, the ultimate tensile strength (UTS), yield strength (YS) and Young's modulus (E) increased, and with more than 5 wt.% CPP addition, UTS, YS and E decreased (FENG; HAN, 2011). This investigation shows that the improvement of mechanical properties is possible, even though it is limited to 5 wt.% of CPP reinforcement, Figure 9.

Feng and Han (FENG; HAN, 2011) also reported that voids due to agglomeration of CPP particles on magnesium matrix were observed. These voids are a probable reason for the decrease in mechanical properties with more than 5 wt.% CPP. The clustering may also lead to

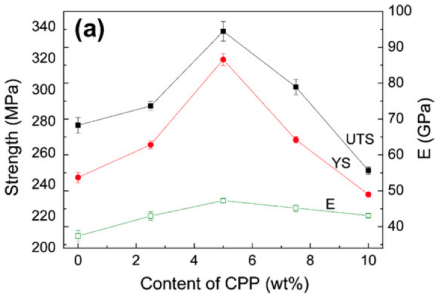

Figure 9 – *Ultimate tensile strength, yield strength and Young's modulus for ZK60 magnesium alloy and ZK60/calcium polyphosphate composite up to 10 wt.% reinforcement. (FENG; HAN, 2011)*

grain boundary embrittlement and decrease in mechanical properties (FENG; HAN, 2011). This may be the reason why the material investigated in the first publication (FENG; HAN, 2010) has poor properties, compared with the latter.

Witte et al. (WITTE et al., 2007) investigated a very similar composite reinforced with hydroxyapatite. The investigated material was AZ91 alloy (Mg-9Al-0.6Zn-0.2Mn) and AZ91 reinforced with 20 wt.% of hydroxyapatite. A higher tensile yield strengh was achieved for the composite compared with the AZ91 alloy, Figure 10.

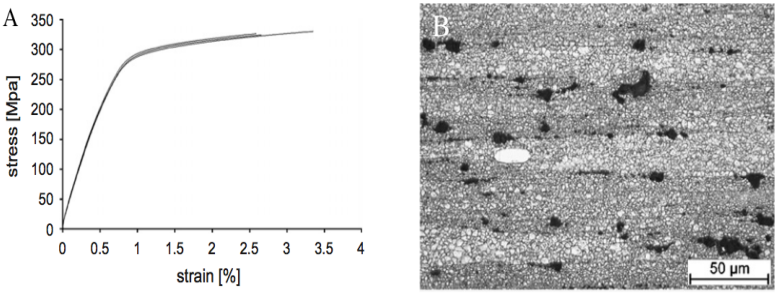

Figure 10 – *Tensile strength of three AZ91-HA composites with 20 wt.% reinforcement (a) and its micrograph showing how particles are distributed in the AZ91 matrix (b). (WITTE et al., 2007)*

3.4.2 Corrosion properties

One of the reasons HA was chosen is its function in the human body and how it interacts within the human tissue (see Section 3.3). The main role of HA is the control of biodegradation, which is successfully achieved even when a small amount is added (FENG; HAN, 2011).

Pardo et al. (PARDO et al., 2009) investigated the corrosion behaviour of silicon carbide reinforced AZ92 composite (up to 10% in volume). Tiwari (TIWARI; BALASUBRAMANIAM; GUPTA, 2007) conducted similar work, but with pure magnesium with up to 16 vol.% of reinforcement. Even though magnesium reinforced with silicon carbide particles exhibit satisfactory mechanical properties (indicated in Section 3.4.1), their corrosion resistance is very poor.

Both investigations (TIWARI; BALASUBRAMANIAM; GUPTA, 2007; PARDO et al., 2009), show that when SiC particles are added to magnesium matrix, the corrosion properties deteriorate. In the first work, the corrosion protect on layer of the composite cracks with the exposure time, giving rise to further corrosion. The low corrosion resistance is also explained by the SiC particle/matrix interface, which breaks the continuity of magnesium, thus inducing localized corrosion (PARDO et al., 2009). In the latter investigation (TIWARI; BALASUBRAMANIAM; GUPTA, 2007), similar results were achieved. The polarization curves for the composites are shown in Figure 11, from which polarization resistance was obtained. These are of 9.11 Ω.cm, 8.53 Ω.cm and 3.43 Ω.cm for Mg, Mg-6SiC and Mg-16SiC respectively. It was also reported (TIWARI; BALASUBRAMANIAM; GUPTA, 2007) that the corrosion layer (probably $Mg(OH)_2$) was easily detached from its surface.

Magnesium matrix composites reinforced with alumina nanoparticles showed good mechanical properties (section 3.4.1). However, the corrosion resistance remained unchanged or worsened. Many investigations on alumina-particle reinforced composites do not report information on corrosion. The corrosion behaviour of a 20 wt.% alumina fiber reinforced AS41 magnesium alloy was reported by Bakkar and Neubert (BAKKAR; NEUBERT, 2007), from which a hypothesis can be made. They show that addition of alumina did not improve corrosion properties and no noticeable corrosion between matrix and fibers was observed. Polarization tests in 0.03 wt.% NaCl, Figure 12, show a quasi-passive behaviour. When the potential increases, the anodic current also increases, until the current density shows a rapid increase without a similar change in the potential. This change is the break-

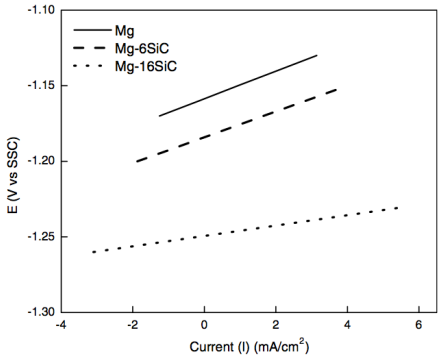

Figure 11 – *Linear polarization plots for Mg, Mg-6SiC and Mg-16SiC in 1 M NaCl. (TIWARI; BALASUBRAMANIAM; GUPTA, 2007)*

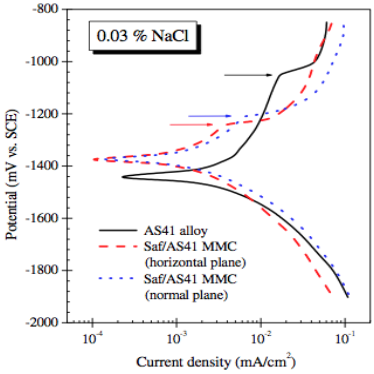

Figure 12 – *Potentiodynamic polarization for AS41 magnesium alloy and AS41 alumina reinforced composite in 0.03 wt.% NaCl solution (BAKKAR; NEUBERT, 2007).*

down potential for the quasi-passive film $Mg(OH)_2$ on sample's surface, which is less resistant with alumina addition, indicated by the arrows. In harsher environments (solutions with 0.3, 1 and 3 wt.% NaCl), the quasi-passive behaviour is absent.

Witte et al. (WITTE et al., 2007) investigated the corrosion behaviour of a Mg-HA composite using the AZ91 Mg alloy. The composite is more corrosion resistant than AZ91, which showed deeper pitting

corrosion. The composite exhibited more uniform corrosion, compared with the unreinforced alloy following exposure to sea water, Figure 13. Feng and Han (FENG; HAN, 2010) showed that weight loss is higher in the base alloy compared with the composites in simulated body fluid (SBF), Figure 14. The investigation with up to 10 wt.% reinforcement by Feng and Han (FENG; HAN, 2011) indicated better corrosion behaviour with the increased volume fraction of CPP as illustrated by the weight loss plots for specimens immersed in opened air physiological saline solution at 37°C, Figure 15. The previous research shows that it is possible to decrease the corrosion rate and achieve uniform corrosion by adding calcium polyphosphate particles, e.g. hydroxyapatite.

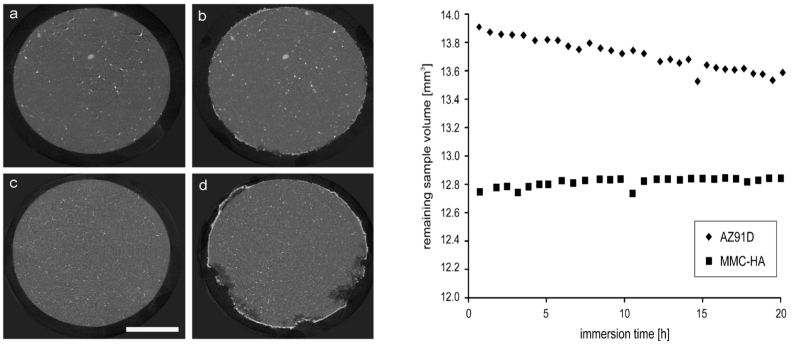

Figure 13 – *Respectively shown AZ91/hydroxyapatite and AZ91 alloy macrographs before (a, c) and after (b, d) immersing in artificial sea water for 20 hours (scale bar = 1 mm). The plot of remaining volume with time is also shown. (WITTE et al., 2007)*

3.5 MECHANICAL ALLOYING

It is a processing route, in which by meanings of constant impact involves cold welding, fracture and rewelding of alloy particles of the two or more constituents which are mixed (LIU et al., 2013). Results depend on material and process parameters, such as powder composition, time, speed, ball-to-powder weight ratio (bpr) and atmosphere. These are discussed in the next Sections.

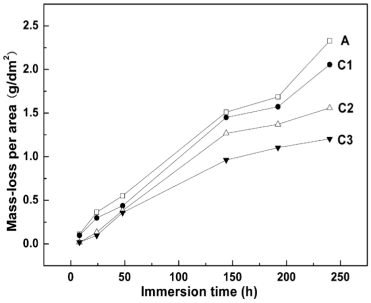

Figure 14 – *Weight loss per area of ZK60 and the composites with 10 wt.% CPP (C1), 20 wt.% CPP (C2) and 30 wt.% CPP (C3). The test was carried out up to 240 hours. (FENG; HAN, 2010)*

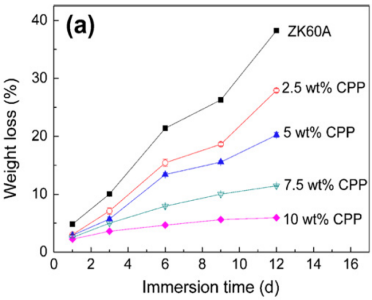

Figure 15 – *Weight loss of ZK60 and ZK60/CPP composites after immersing in physiological saline for 1 to 12 days. (FENG; HAN, 2011)*

3.5.1 Types of mills and its implements

Different types of mills differ in capacity, efficiency of milling and other working conditions as cooling and heating (SURYANARAYANA, 2001). The planetary ball mill, which was used in this work, is introduced as follows.

- In a planetary ball mill, over some hundred grams of material can be milled each time. Its name is based on the crucible's movement. It is a planet-like movement, i.e. rotational and translational movement relative to its central axis. The rotational move-

ment is in the opposite direction to the translational movement. This leads the centrifugal forces to work in opposite directions and the balls to come in contact with the walls of the vessel inducing friction. The resultant impact and its effect is shown in Figure 16. (SURYANARAYANA, 2001)

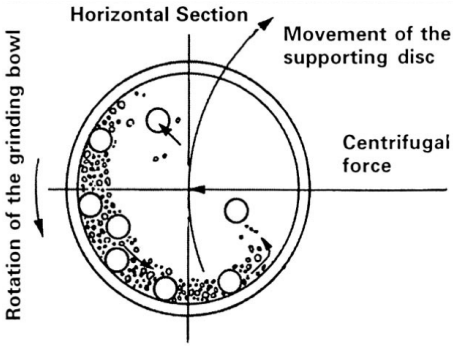

Figure 16 – *Illustration of material and ball motion along the crucible, depicting the opposite directions of translational and rotational movements. (SURYANARAYANA, 2001)*

3.5.2 Material behaviour during ball-milling

The material in high energy ball milling undergoes severe changes due to high energy impact. When balls collide, powder traps between them, Figure 17. This leads to plastic deformation, giving rise to work hardening of the powder, followed by fracture. Welding may also occur, increasing particle size, which is significant in the early stages, as the particles are still soft and tend to weld together (in case of ductile-brittle or ductile-ductile material combination). After these stages, particles tend to have a layered structure, which is schematically in Figure 17. (SURYANARAYANA, 2001)

There are three different types of milling, based on types of powder being used. Those are ductile-ductile, ductile-brittle and brittle-brittle. The present work uses magnesium metallic chips and hydroxyapatite powder. The metallic chips are relatively ductile compared with the hydroxyapatite particles and ball milling of metallic chips with hydroxyapatite is ductile brittle type of milling.

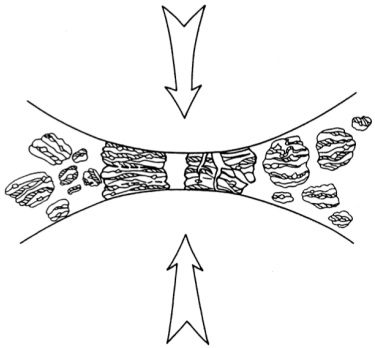

Figure 17 – *Balls' collision showing powder particles in between. (SURYANARAYANA, 2001)*

When hard particles are smashed by colliding balls, they fracture, unlike ductile particles, which are flattened, Figure 18. The fragmented brittle material tend to be engulfed by the ductile powder, forming a layered structure, shown in Figure 19a. Once the material became more brittle with work-hardening by further milling, lamellae are refined with additional particle break-up, 19b. After the particles and lamellae are further refined, a better dispersion of the brittle material within the ductile matrix is achieved (if they are not soluble into each other), Figure 19c. (SURYANARAYANA, 2001)

3.5.3 Other processing routes

Many techniques for manufacturing Mg composites were already reported, such as stir casting (WANG et al., 2014) and hot extrusion posteriorly to mixing and compressing the powders (FENG; HAN, 2011). Previous lab investigations evidenced that the formation of hazardous gases containing PH_3 when hydroxyapatite is in contact with molten magnesium. This gas is highly toxic and can cause serious health problems.

After mixing the powders with magnesium a poor particle distribution was observed with a poor interface between matrix and particles. When the material is extruded directly after mixing, mechanical and corrosion properties deteriorated compared with the extruded base alloy (FENG; HAN, 2011).

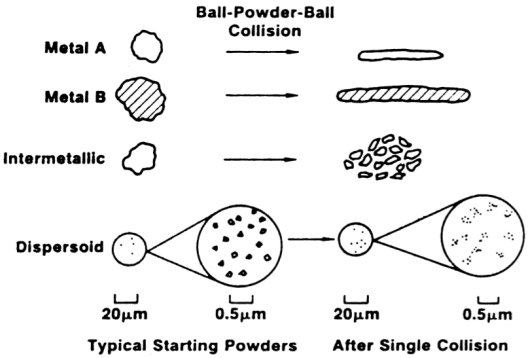

Figure 18 – *Representative material behaviour during mechanical alloying. (SURYANARAYANA, 2001)*

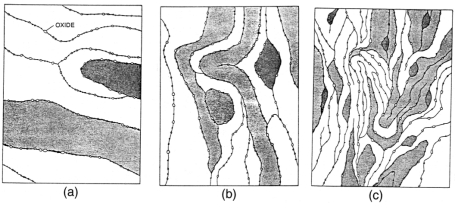

Figure 19 – *Microstructural evolution of ductile-brittle mechanical alloying. (SURYANARAYANA, 2001)*

Due to these reasons, mechanical alloying is the only possible and effective method capable of producing such composite.

3.5.4 Milling variables

There are several variants in ball milling. The most important variants are discussed in this Section, which are speed, time and ball-to-powder ratio. These are controlled and determined, based on the materials and processing constraints. Atmosphere is a relevant variant but it is relatively difficult to control the atmosphere.

3.5.4.1 Speed and temperature

Speed is one of the most important variables in mechanical alloying. When it is increased, more collisions occur and therefore, more energy is put into the system. However, depending on mill's design, there are restrictions on speed. Above a critical speed, the centrifugal forces are too high, pinning balls to the wall and not exert any impact on the material. (SURYANARAYANA, 2001)

Temperature increases with impacts and friction. In some cases, this was an advantage due to diffusion triggered by temperature, which allows for a better distribution of particles and any alloying additions. However, it can also be a disadvantage, specially if temperature increases substantially, which may contaminate the mixture. (SURYANARAYANA, 2001)

Temperature increase can lead to exothermic reactions in the materials to be milled (SURYANARAYANA, 2001).

3.5.4.2 Ball-to-powder weight ratio

Even though ball-to-powder weight ratio (bpr) also influences the results, sometimes bpr is chosen according to mill's capacity. Normally, ratios of 10:1 are used in small capacity mills, while in high capacity mills, ratios of 50:1 or even 100:1 can be used. It is one of the main parameters that influence the milling time, because higher the bpr, higher the energy involved in the process, as more impacts occur. Figure 20 shows particle size achieved after milling for a given time, by changing the bpr. More energy is involved with higher ball-to-powder ratios, giving rise to smaller particle size, after a given milling time. (SURYANARAYANA, 2001)

3.5.4.3 Milling time

Time is the most important parameter. Different mills and other variants such as temperature, bpr and milled material will have substantial influence on the time required to achieve a given particle size. Thus, time must be chosen in accordance with above parameters. There is also an certain amount of time with which results are optimized, as longer times can lead to contamination or the formation of embrittling phases. Therefore, one must not mill the material for longer times than

necessary. (SURYANARAYANA, 2001)

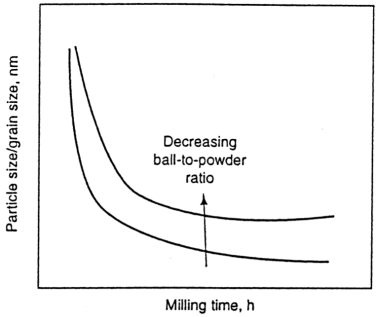

Figure 20 – *Curves of particle refinement after given milling time, considering different ball-to-powder ratios. (SURYANARAYANA, 2001)*

3.5.4.4 Milling atmosphere

The consequence of wrong atmospheres is the contamination. The vessel can be filled and sealed inside a glovebox with argon, reducing contamination risks. Other gases can also be used, as well as cryogenic environments to induce brittle behaviour of ductile materials and to achieve among other results, finer particles. The presence of normal atmosphere can lead to the formation of oxides and nitrides, specially if the powders are reactive, giving rise to the formation of unexpected compounds. (SURYANARAYANA, 2001)

3.6 HOT EXTRUSION

Magnesium extrusion is similar to that employed for other metals and can be direct or indirect. In the first, a ram pushes the material to be extruded over a stationary die, Figure 21(a). In the latter, both die and container move towards the material to be extruded, Figure 21(b). Containers, ram and other used tools are preheated with the material to avoid temperature decrease in the material and extruder. Processing temperature depends on the alloy and final shape, ranging from 300 to 450°C. Care must be taken with temperature, as friction between the ram, die and the material can substantially increase the

temperature during extrusion. If the temperature exceeds solidus temperature of the alloy, hot cracking can appear on the extruded surface. Generally, extruded magnesium has satisfactory mechanical properties due to refinement in the microstructure. However, heat treatments are sometimes needed to refine and homogenize its microstructure after hot extrusion. (AVEDESIAN; BAKER et al., 1999)

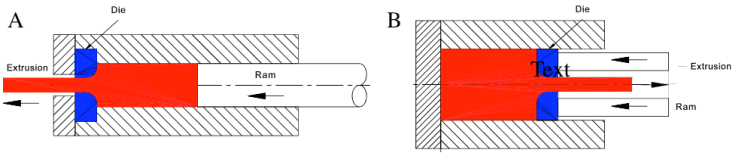

Figure 21 – *Illustration of direct (a) and indirect (b) extrusion processes. (WWW.SUBSTECH.COM, 2014)*

4 MATERIALS AND METHODS

4.1 MATERIALS

4.1.1 Magnesium alloy

The alloy used is the commercially available ZK60. The ingots were cast and then machined in order to obtain small particles for mechanical alloying. One of the machined ZK60 ingots is shown in Figure 22.

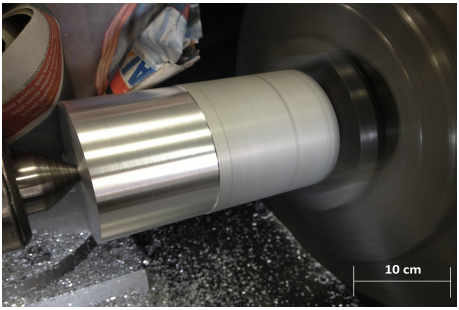

Figure 22 – *Magnesium ingot being machined.*

4.1.2 Hydroxyapatite

The hydroxyapatite ($Ca_{10}(PO_4)_6(OH)_2$) was bought from Alfa Aesar GmbH, Germany and has a nominal size $<42\mu$m.

4.2 PROCESSING

4.2.1 Ball milling

Ball milling was performed to incorporate HA particles into the magnesium matrix, using a Retsch PM 100 high energy ball mill, Figure 23. Here, stainless steel crucible and balls were used. Therefore, balls

and vial walls were coated with ZK60 before milling the composite to decrease the contamination risk. The coating was done by milling only ZK60 base alloy at 350 rpm for 2 minutes.

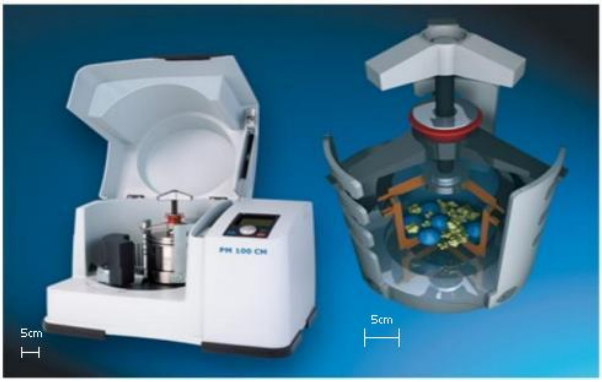

Figure 23 – *Retsch PM 100 ball mill and its operational outline.*

For mechanical milling, a quantity of spheres that fill up to half of the crucible's volume was weighed. From this value, material mass was calculated according to the selected ball to powder ratio. Vessel was then filled with the balls and the material to be milled. Afterwards, the vessel was closed and fixed inside the mill and milled at a given speed and time.

The parameters have a great influence in the final composite microstructure. In a previous study, composite's mechanical alloying variants - speed, ball to powder ratio (bpr) and revolutions per minute (rpm) - were varied to find the optimised conditions (STÜPP, 2013). After long time experiments, up to 90 h (see Table 2), parameters 5, 6 and 7 were selected for further investigation. Finally, parameters corresponding to sample 5 were chosen for powder production. Mechanical milling was then conducted for 7 h, with a bpr of 20:1 and speed of 250 rpm.

4.2.2 Hot extrusion

After the powder was mixed and HA particles distributed into the magnesium matrix by mechanical alloying, the mixture was hot extruded. A vertical extruder was used, Figure 24, where the green

Table 2 – Ball milling experiments of pure magnesium with 20 wt.% hydroxyapatite composite samples.

Sample	Ball to powder ratio (bpr)	Speed (rpm)	Time (h)
1	5:1	200	90
2	5:1	250	40
3	5:1	250	20
4	5:1	250	10
5	20:1	250	7
6	5:1	250	5
7	20:1	250	2

arrow indicates the extrusion direction.

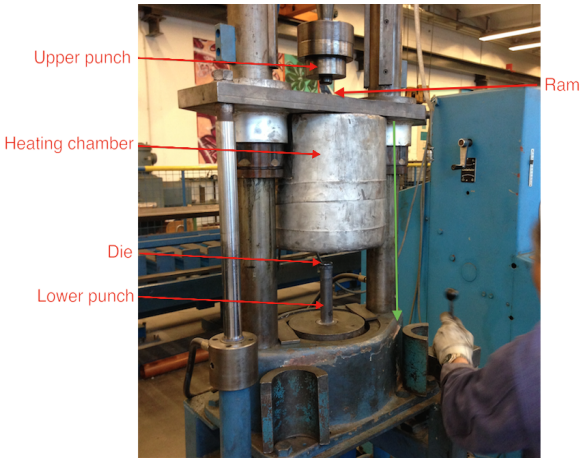

Figure 24 – *Vertical extruder and its components.*

The material, dies and punches were preheated at 270 - 280°C, while the machine's heating chamber was kept at 240°C during extrusion. After reaching uniform preheating temperature, dies and punches were carefully mounted in the machine, the powder poured into the 30 mm diameter die and extruded indirectly. The parameters used for extrusion are shown in Table 3. The extrusion for the material with 20 wt.% hydroxyapatite was performed at a lower speed (3 mm/s), due to heat generation. The last 30 mm was extruded using direct extrusion

due to the end of the extruder's path. This is the reason for the force to range from 16 to 32 ton. Indirect extrusion needs less force, which must be increased by a factor of two when direct extrusion takes place.

Magnesium rods of approximately 1000 mm x 9.5 mm were extruded. From the extruded material, a length of 10 mm at the top and bottom was discarded, due to end effect associated with the extrusion. The specimens for compression, tensile and corrosion tests were machined from the extruded bars.

Table 3 – Extrusion parameters for manufacturing the composites.

Parameter	Value
Powder temperature	270 - 280°C
Extruder temperature	240°C
Extrusion ratio	9.97
Speed	8.5 - 9.0 mm/s
Force	16 - 32 ton
Specimen's length	1000 mm
Specimen's diameter	9.5 mm

4.2.3 Specimens fabrication

For mechanical and corrosion tests, five specimens for each test were machined from the extruded rods. Figure 25 shows tensile and compression specimens in details. DIN 50125 standard was used for tensile tests. For compression tests DIN 50106 standard was used. The specimens for corrosion investigation were 8.5 mm in diameter and 3 mm in thickness.

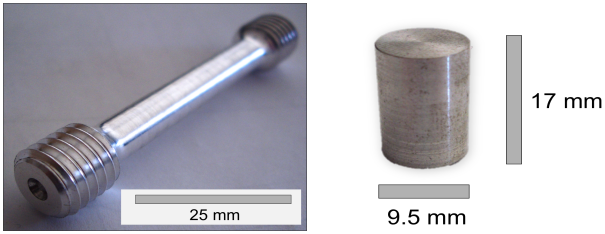

Figure 25 – *Tensile and compressive specimens respectively.*

4.3.1 Optical microscopy (OM) and scanning electron microscopy (SEM)

Both light and scanning electron microscopy were used in this study. The optical microstructures of the composites were characterized with a Reichert-Jung MeF3 light microscope. Further microstructural examinations were then conducted with a Tescan VEGA 3 scanning electron microscope operating at 15 kV in the high vacuum setting. For corroded samples the low vacuum mode with a pressure of 5 Pa was used.

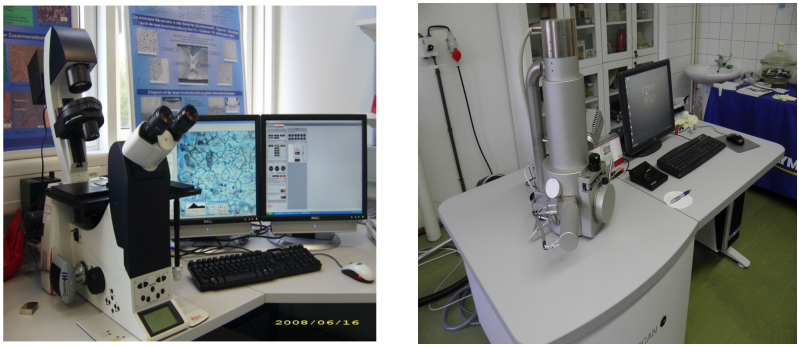

Figure 26 – *Reichert-Jung MeF3 optical microscope (left) and Tescan VEGA 3 scanning electron microscope (right). (WWW.FORTECH.ZCU.CZ, 2014)*

The Tescan VEGA 3 SEM is also equipped with energy dispersive X-ray spectroscopy (EDXS) for chemical analysis. The software used for analysing particle and grain sizes of the microstructure was "analySIS pro 5.0" from Olympus.

The optical microstructure was observed after ball milling on the milled power and the bulk composite rods after extrusion. The extruded specimens were examined both in longitudinal and cross section to the extrusion directions. Samples for optical microscopy were embedded in epoxy, ground with Emery paper (from 500 to 2500) and polished with water-free colloidal silica solution with particle size 50 nm for 15 minutes. The samples were etched in a solution composed

of ethanol (70 wt.%), picric acid (8-9 g), distilled water (20 vol.%) and acetic acid (5 vol.%). After both polishing and etching, samples were cleaned with ethanol and dried with hot air.

Samples for SEM analysis were prepared as for optical microscopy, but were not etched. For the examination of the planner view corrosion layer of the corroded samples and mechanically tested samples no preparation was done prior to SEM examination.

4.3.2 X-Ray diffraction (XRD)

A Siemens D5000 X-Ray diffractometer was used for X-Ray characterization of the bulk material after ball milling and extrusion, Figure 27. The samples were measured with Cu K_α radiation at a voltage of 40 kV and current 40 mA. A step size of 0.01 and a dwell time of 10 s was used to measure the diffraction of the sample in the 2 theta range 10-80. The crystal structure information for characterizing various phase observed was "Pearson's Crystal Data - crystal structure database for inorganic compounds - version 1.6".

The XRD was performed for every sample after hot extrusion and mechanically alloyed powder. In order to determine the corrosion products in the corrosion layer, a D8 advance XRD reflectometer from Bruker was used.

4.3.3 Density and porosity

Porosity was estimated by calculating density and comparing that with the theoretical density of the composite. The latter was calculated with Equation 4.1, where M_{total} is the composite's total mass, %HA and %ZK60 are the respective mass fractions of HA and ZK60, and ρ their respective density. A perfect interface particle-matrix was considered for density calculations. Porosity is calculated with Equation 4.2.

$$\rho_{\text{composite}} = \frac{M_{\text{total}}}{\frac{\%_{\text{HA}} \cdot M_{\text{total}}}{\rho_{\text{HA}}} + \frac{\%_{\text{ZK60}} \cdot M_{\text{total}}}{\rho_{\text{ZK60}}}} \tag{4.1}$$

$$\%_{\text{pores}} = (1 - \frac{\rho_{\text{material without pores}}}{\rho_{\text{material}}}) * 100 \tag{4.2}$$

Figure 27 – *Siemens D5000 X-Ray diffractometer.*

4.4 MECHANICAL PROPERTIES

4.4.1 Tensile and compression testing

For both tensile and compression tests, a Zwick Z050 universal testing machine was used and 5 specimens for each test were performed. An extensometer was used for a precise measurement of the specimens' elongation or compression. Machine's specifications are shown in Table 4 and a scheme in Figure 28, while the test parameters are shown in Table 5. Pre-force is applied, so that the material is not loose in between the clamps.

Table 4 – Universal Testing Machine Zwick Z050 specifications.

Maximal force	50 kN
Transverse speed	0.001 - 400 mm/min
Temperature	RT - 250°C

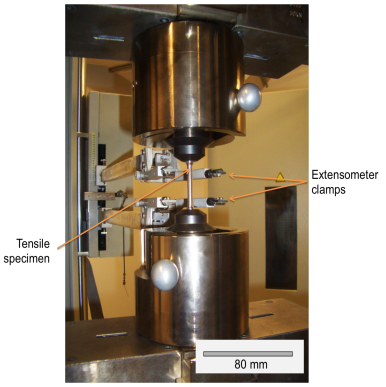

Figure 28 – *Testing area of a Zwick Z050 universal testing machine.*

Table 5 – Compression and tensile tests parameters.

Maximal force	48 kN
Pre-force	2 MPa
Speed pre-test	10^{-2} s^{-1}
Strain rate	10^{-3} s^{-1}
Temperature	25°C

4.4.2 Hardness

The hardness was measured for the composites after extrusion. A M1C010 universal hardness testing machine from EMCOTEST was used with HV 5 (indenter's size related hardness scale). The machine is shown in Figure 29.

Samples prepared longitudinal and cross section to extrusion directions were characterized. Samples were ground with SiC paper up to 2500. A minimum of 10 measurements were made for each samples, as shown in Figure 30.

4.5 CORROSION TESTING

The corrosion behaviour was evaluated with immersion and potentiodynamic polarization measurement using a DMEM (Dulbecco's

Figure 29 – *EMCOTEST M1C010 universal hardness testing machine. (WWW.TUCHEMNITZ.DE, 2014)*

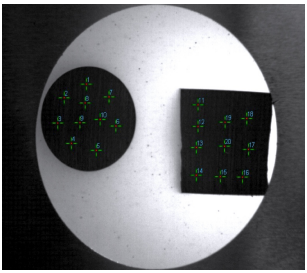

Figure 30 – *Hardness indentations for cross section (left) and longitudinal (right) to extrusion.*

Modified Eagle Media) solution with Glutamax containing 10% fetal bovine serum (FBS). The composition of DMEM solution is provided in the Table 6. A buffer system composed by sodium bicarbonate (3.7 g/l) is used, that requires a 5% CO_2 containing storage room, otherwise the pH increases. When exposed to ambient levels of CO_2, DMEM becomes basic very rapidly. (WWW.LIFETECHNOLOGIES.COM, 2014) FBS is the remainder after blood coagulation, after centrifugation to remove red blood cells. It is the most used cell culture medium due to low level of antibodies and high concentration of growth factors. It contains a variety of proteins, allowing cells to grow, survive and divide (JOCHEMS et al., 2002). Osmolality of the solution after immersion was measured with an Osmomat auto, which compares water with other solution's freezing point. Here, water has a freezing point of 0°C and a random

solution with saline concentration of 1 osmo/kg has a freezing point of -1.858 °C. An automatic pH meter was used to measure pH of the solution.

Table 6 – Composition of DMEM solution.

DMEM (mg/l)	
$CaCl_2$ (water free)	200
$Fe(NO_3)_3$. $9H_2O$	0.10
KCl	400
$MgSO_4$ (water free)	97.67
NaCl	6400
NaH_2PO_4 . H_2O	125
$NaHCO_3$	3700
D-Glucose	4500
Phenolrot	15
Natriumpyruvat	110
Aminoacids	–
Vitamins	–
pH	7.0 - 7.4

The immersion corrosion experiments were conducted in DMEM + FBS solution, which was naturally-aerated and had an initial pH of 7.0-7.4 that changed during the experiments, at a temperature of 37°C. Electrochemical tests were conducted with Hank's solution (composition shown in table 7) and DMEM + FBS at 37°C. The Hank's solution was naturally-aerated and had a pH of 7.8. The composition of the Hank's solution is provided in Appendix B. Samples were sterilized by autoclaving for 20 minutes at 121 °C. Both sterile and non-sterile samples were investigated with electrochemical tests.

4.5.1 Immersion

For immersion experiments, only autoclaved samples were used. They were immersed separately in 3 ml of solution. The material was kept in an incubator, which parameters follow in Table 8. After immersion, pH was measured and 50 μl of solution for each specimen was taken for osmolality measurement. Samples were cleaned with distilled water and dried for 24 h in another incubator, in which the temperature is 50°C. SEM and XRD were carried out to analyse the corrosion prod-

Table 7 – Composition of Hank's solution.

Hank's solution (g/l)	
NaCl	8
KCl	0.4
$CaCl_2$	0.14
$NaHCO_3$	0.35
$MgSO_4$. $7H_2O$	0.2
NaH_2PO_4 . H_2O	0.06
NaH_2PO_4	14
pH	7.8

ucts after immersion. Samples were then immersed in chromic acid for 10 minutes each side, which removed the corrosion products. Weight loss was calculated by weighting samples before immersion tests and after corrosion products were removed. Corrosion rate (CR in mm/year) was calculated from Equation 4.3, where W is the weight loss (g), ρ is density (g/cm^3), A is sample's area (cm^2) and t the immersion time (h).

$$CR = 87.6.10^4.\frac{W}{\rho.A.t} \tag{4.3}$$

Table 8 – Incubator parameters for immersion tests.

Temperature	37°C
CO_2	5%
O_2	20%
Humidity	96%
Time	72 h

4.5.2 Potentiodynamic polarization

Electrochemical measurements were conducted using a Gill AC computer-controlled potentiostat both in sterile and non-sterile specimens. For the first, experiments both in Hank's and DMEM + 10 vol.% FBS solutions were made. Potentials were measured with respect to

Ag/AgCl reference electrode. A platinum foil was used as the auxiliary electrode. Polarization studies were carried out starting at -150 mV relative to open-circuit potential (OCP - measured after 1h of immersion) at a sweep rate of 0.2 $mV.s^{-1}$ until the anodic branch reaching a final current density of 1 $mA.cm^{-2}$.

For the correct E_{corr} and i_{corr} measurements using the Tafel extrapolation method, only the cathodic branch of the polarization curve is used. The anodic polarization curve of magnesium does not satisfy the Tafel law because hydrogen evolution and dissolution of Mg occurs simultaneously during the corrosion of magnesium (ZENG et al., 2011). That is why the anodic branch of the polarization curve is most of the times with noises and then the cathodic branch is used for measuring the E_{corr} and i_{corr} in Mg by the Tafel extrapolation method. (ZENG et al., 2011)

5 RESULTS

5.1 MAGNESIUM AND HYDROXYAPATITE

Particle size of Mg after machining was in millimeters scale. HA particle size was measured before mechanical alloying and found to be less than 41 μm, Figure 31.

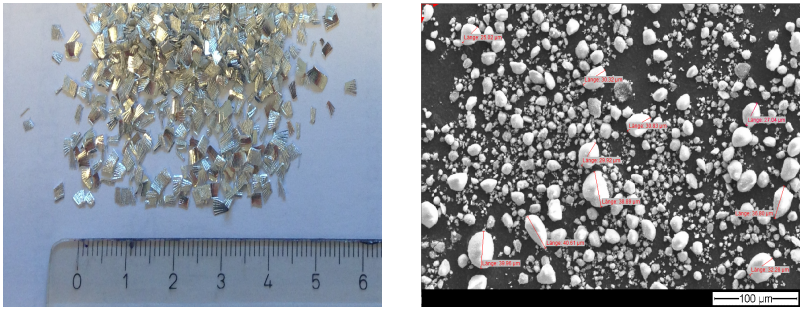

Figure 31 – *Magnesium chips used for mechanical alloying (left) and scanning electron microscope's image evidencing hydroxyapatite particle size (right).*

Before ball milling, XRD of the HA powder was performed, which is shown in Figure 32. From this XRD, it is possible to later identify the peaks for this constituent in the composites.

5.2 BALL MILLING

5.2.1 Light microscopy

The microstructure analysis of samples milled for 20, 7, 5 and 2 h (Table 2) are shown in Figure 33. In this case specimens were not etched after ball milling. The bright part in the sample is magnesium matrix where HA was not detected. The HA particles are the black points in the matrix.

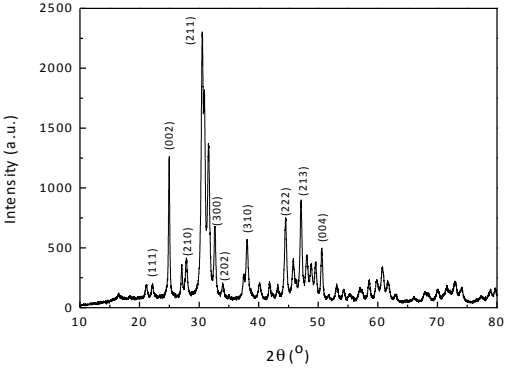

Figure 32 – *XRD for HA powder.*

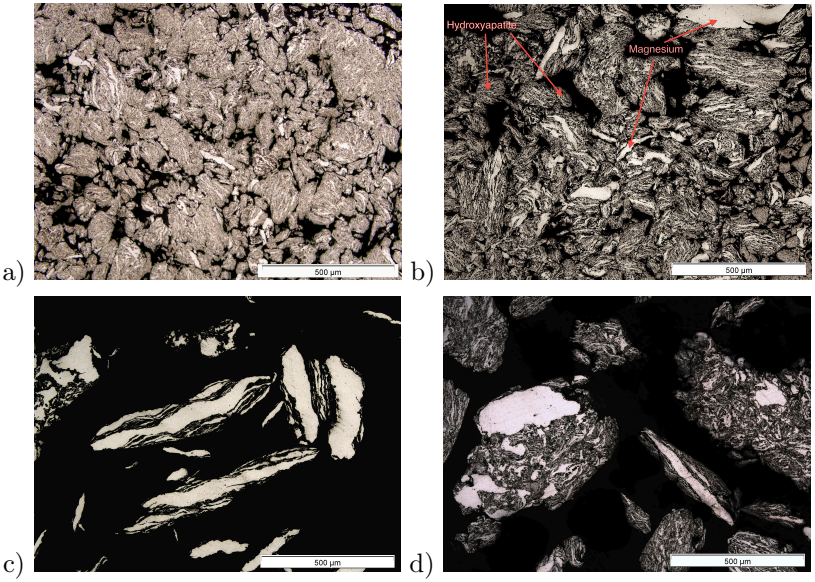

Figure 33 – *Micrographs of samples 3(20 h, bpr 5:1, 250 rpm), 5(7 h, bpr 20:1, 250 rpm), 6(5 h, bpr 5:1, 250 rpm) and 7(2 h, bpr 20:1, 250 rpm).*

5.2.2 Scanning electron microscopy (SEM) and energy dispersive spectrometry (EDXS)

Samples 5, 6 and 7 after ball milling were analysed in the SEM to confirm the distribution of HA. Figure 34 shows both microstructure and Ca map for each sample. As Ca is the major constituent of HA, this method is used to determine the distribution of HA. Therefore, HA can be observed and it was possible to assume that the white particles in the micrographs were in fact HA. The sample 6 has the poorest distribution of Ca compared with the other milling conditions.

5.3 EXTRUSION

The micrographs recorded along the extrusion direction are shown in Figures 35 and 36. The HA (as black particles) was visible within the magnesium matrix. In the extruded specimens, the particle distribution followed the same trend as the milled powder. Etched specimens in Figures 37 and 38 show the grain sizes, along with the distribution of grain sizes throughout the sample, determined by the distribution and quantity of HA.

The microstructures contain a duplex distribution of grains with regions of large grains surrounded by fine grains. The large grained regions occur along the extrusion direction. With the addition of HA, regions of coarse grains decreased and only small regions of coarse grains are observed in ZK60-20. The coarse grain size also decreased with the increase in HA content. In ZK60, ZK60-7.5 and ZK60-10, these grains range from 15 μm to 40 μm, while in ZK60-20, they are less than 20 μm. The fine grained region contained grains that are less than 1 μm. HA is homogeneously distributed throughout the samples, and this distribution causes the formation of fine grains. In ZK60 alloy the fine grained regions are due to the presence of oxide particles introduced during machining and ball milling.

5.3.1 X-Ray diffraction (XRD)

XRD was performed to evaluate constituents of the mechanically milled and extruded composite. Figure 39 shows the composites and the based alloy XRD patterns. In alloy extruded samples, Mg and $MgZn_2$ can be observed. In the composites diffraction, HA is also observed.

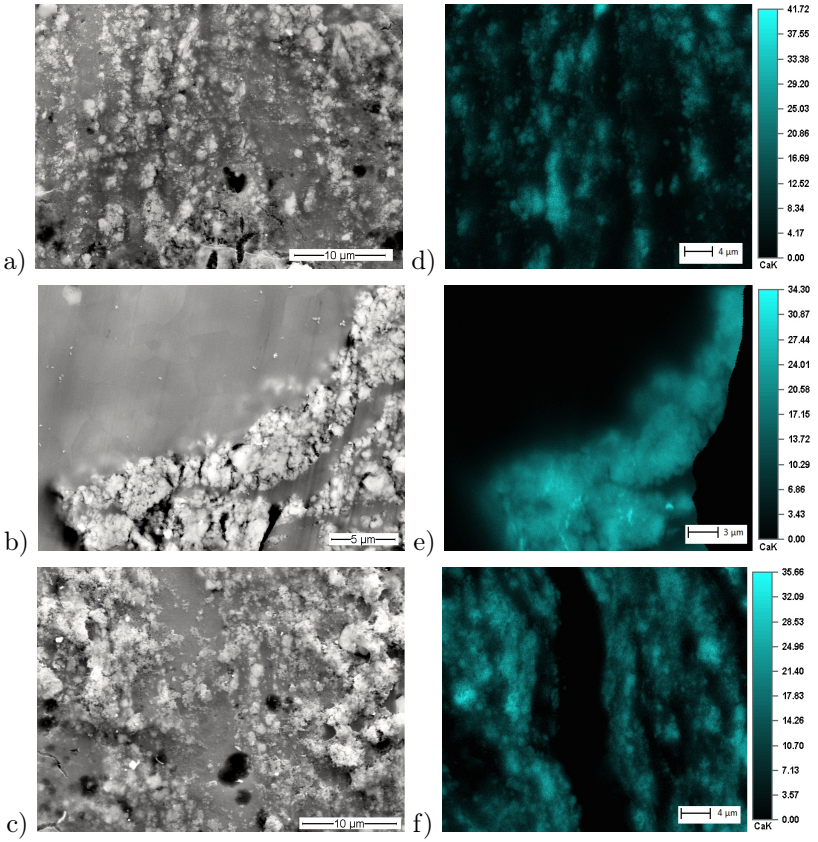

Figure 34 – *SEM micrographs (a, b, c) and EDXS (d, e, f) for samples 5(20:1 bpr, 250 rpm, 7 h), 6(5:1 bpr, 250 rpm, 5 h) and 7(20:1, 250 rpm, 2 h).*

5.3.2 Density and porosity

The theoretical and calculated densities along with porosity values are shown in Table 9. The composites' density after extrusion are similar to the theoretical values suggesting low levels of porosity.

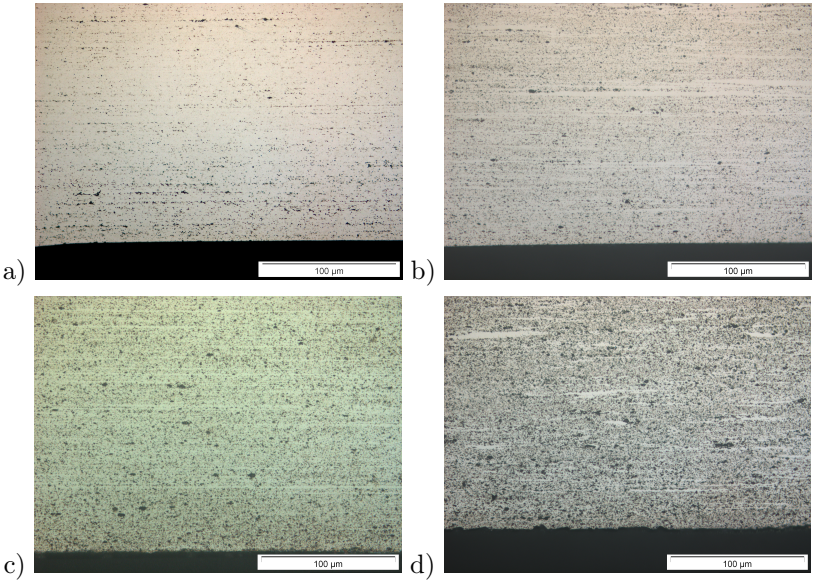

Figure 35 – *Micrographs of longitudinal section in extruded samples ZK60 (a), ZK60-7.5 (b), ZK60-10 (c) and ZK60-20 (d) exhibiting particle distribution.*

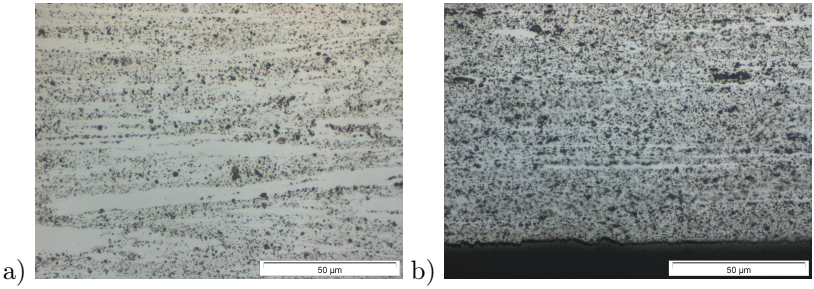

Figure 36 – *Higher magnification of micrographs in longitudinal section of extruded samples ZK60-10 (a) and ZK60-20 (b) exhibiting particle distribution.*

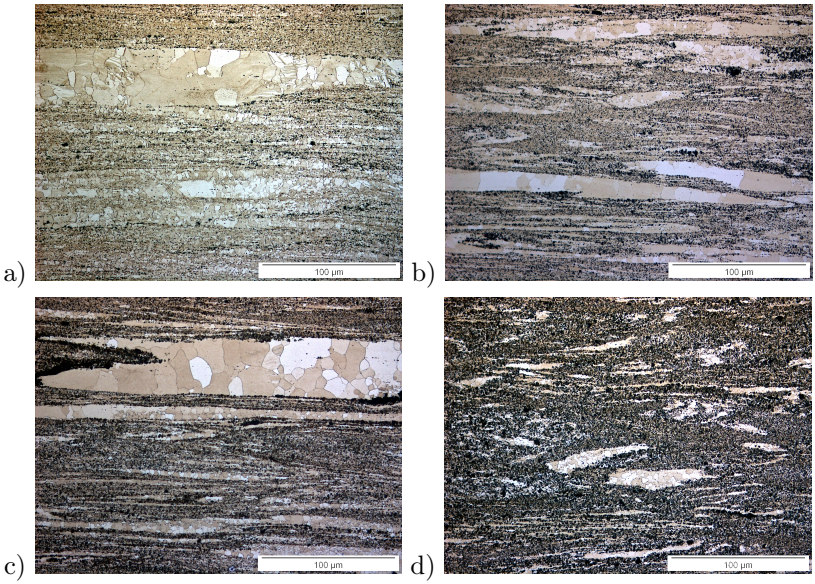

Figure 37 – *Micrographs of longitudinal section in etched extruded samples ZK60 (a), ZK60-7.5 (b), ZK60-10 (c) and ZK60-20 (d) exhibiting grain size distribution.*

5.4 MECHANICAL PROPERTIES

5.4.1 Tensile tests

Tensile stress-strain curves for the base alloy and the composites are shown in Figure 40 with the pertinent information summarized in Table 10. The best elongation to failure was observed for the ZK60 alloy. A large decrease in elongation to failure was observed with the HA addition while the tensile yield strength (TYS) and ultimate tensile strength (UTS) increased. There was no yield stress observed for the ZK60-20 as the sample failed in a brittle manner. For ZK60-20, the curve was moved by 0.2 to the right, so that it was not overlapped by the others. Its features are shown in Table 10.

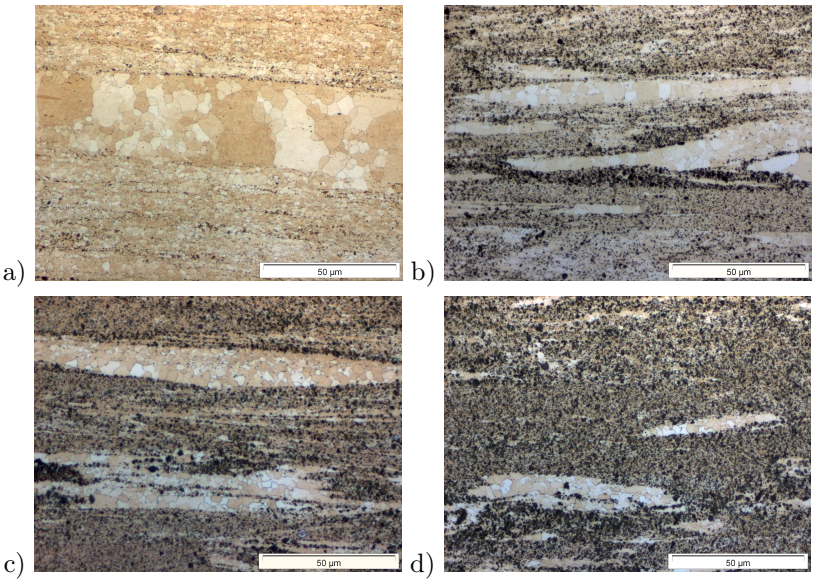

Figure 38 – *Higher magnification of micrographs in longitudinal section of etched extruded samples ZK60 (a), ZK60-7.5 (b), ZK60-10 (c) and ZK60-20 (d) exhibiting grain size distribution.*

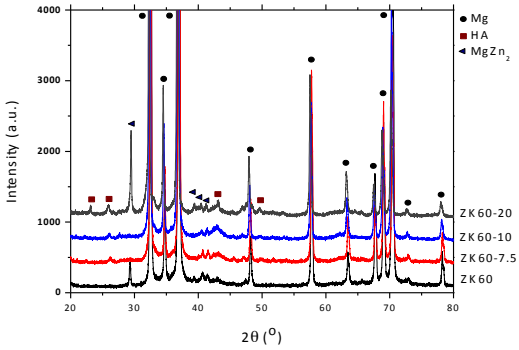

Figure 39 – *XRD patterns for the three different composites and the ZK60 alloy without HA addition.*

Table 9 – Porosity, theoretical and calculated densities (g/cm^3) for the different composites.

Material	Theoretical density	Calculated density
Hydroxyapatite	3.10	–
ZK60	1.83	1.81 ± 0.01
ZK60-7.5	1.89	1.89 ± 0.01
ZK60-10	1.91	1.91 ± 0.01
ZK60-20	1.990	1.990 ± 0.001

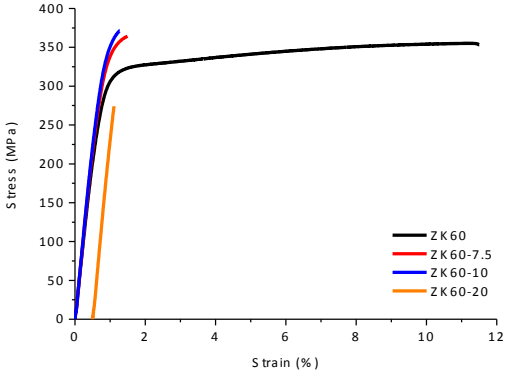

Figure 40 – *Tensile stress - strain curves for the ZK60 alloy and ZK60 with HA.*

5.4.2 Compression

Compression stress-strain curves are shown in Figure 41, and the pertinent features are summarized in Table 11. Ultimate compressive strength (UCS) increased along with compressive yield strength (CYS) when HA is added. The compression values were not very different for the composites, but considerably larger for the base alloy. The increase in the compressive yield strength with HA additions was approximately 80 MPa for ZK60-20, while the UCS increased by approximately 14%. Compression to failure decreased by ∼46% with the addition of 20 wt.% HA still showing a ductile behaviour.

Table 10 – Room temperature tensile properties for the ball milled and extruded composites.

Material	0.2% TYS (MPa)	UTS (MPa)	Elongation (%)
ZK60	288 ± 4	348 ± 5	8.2 ± 2.6
ZK60-7.5	326 ± 11	360 ± 7	0.6 ± 0.2
ZK60-10	344 ± 7	377 ± 5	0.6 ± 0.1
ZK60-20	–	294 ± 30	0.04 ± 0.0

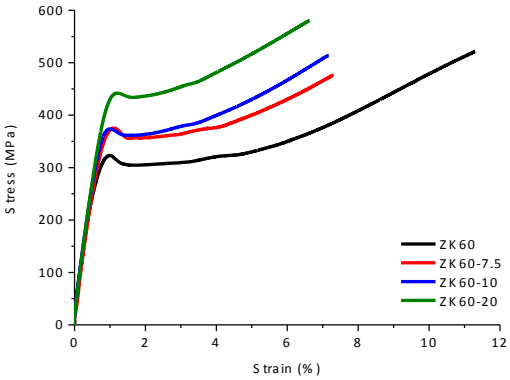

Figure 41 – *Compression stress - strain curves for the ZK60 alloy and ZK60 with HA.*

Table 11 – Room temperature compressive properties for the ball milled and extruded composites.

Material	0.2% CYS (MPa)	UCS (MPa)	Elongation (%)
ZK60	277 ± 22	485 ± 35	9.5 ± 1.0
ZK60-7.5	351 ± 19	520 ± 26	7.2 ± 0.6
ZK60-10	341 ± 20	529 ± 13	6.6 ± 0.4
ZK60-20	356 ± 54	554 ± 20	5.1 ± 0.4

5.4.3 Hardness

Hardness for all samples, both along and cross-section to extrusion direction are shown in Figure 42. The hardness increased with

the addition of HA, and slightly larger values were observed in the longitudinal direction.

Figure 42 – *Hardness values for all samples.*

5.5 CORROSION MEASUREMENTS

5.5.1 Sterilization

The sterilization induced the formation of a black oxide layer on the specimens, Figure 43. This layer was not homogeneous and it contained defects, which might be detrimental to the corrosion behaviour.

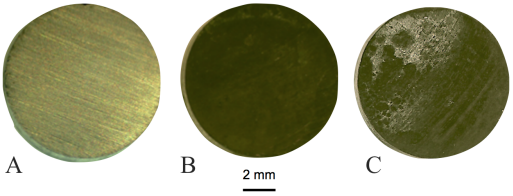

Figure 43 – *Specimens used for corrosion measurements before sterilization (a) and after sterilization, in which a black oxide layer was observed (b), showing defects this layer can present (c).*

5.5.2 Immersion

The pH of the solution before immersion is nominally between 7.0 and 7.4. After 72 h of immersion, this value was different for each composite, 8.05 for ZK60-20 and 8.73 for ZK60.

After immersion, corrosion products were observed on the surface of the material, Figure 44. In order to study the components of the corroded layer in each specimen, XRR (X-ray reflectometry) was performed on the samples used for immersion tests, Figure 45. The diffraction pattern of the corroded composites contained predominantly MgOH and MgO reflections with some Ca_2P_2 phase. HA could be detected in the extruded and corroded specimens containing HA.

Samples were then cut in cross section and analyzed in the SEM and EDXS, Figures 46 and 47. The corrosion layer decreased with the increase in HA content from $\sim$50 μm in ZK60-10. The thickness of ZK60-20 was less than 2 μm. EDXS shows the formation of three different layers, product of corrosion. The outer one based in Mg and O, an intermediate layer composed by Ca and P and the inner layer also composed by Mg and O.

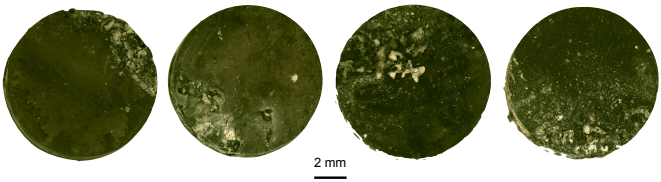

Figure 44 – *Specimens after immersion evidencing the corrosion products on the surface of the material. From left to right, ZK60, ZK60-7.5, ZK60-10, ZK60-20.*

After analyzing the corrosion products, the materials were immersed in chromic acid for corrosion products removal and then cleaned and dried, Figure 48. The corrosion rates calculated from weight loss are listed in Table 12. From these results it can be seen that with up to 7.5 wt.% of HA addition, an increase in the corrosion rate was observed, which began to decrease with more than 10 wt.%, reaching the lowest corrosion rate, for the ZK60-20 composite.

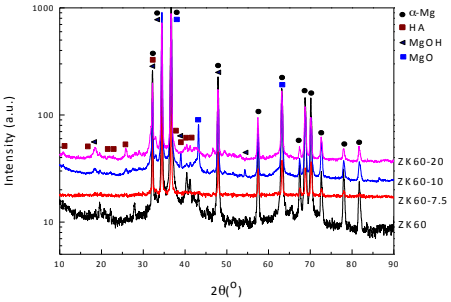

Figure 45 – *XRR showing the corrosion products after immersion.*

Table 12 – Corrosion rate values derived from immersion in DMEM + 10 vol.% FBS.

Material	Corrosion Rate (mm/year)
ZK60	0.49 ± 0.07
ZK60-7.5	0.54 ± 0.01
ZK60-10	0.47 ± 0.12
ZK60-20	0.40 ± 0.19

5.5.3 Potentiodynamic polarization

5.5.3.1 Effect of sterilization by autoclaving

Potentiodynamic polarization curves for sterile and non sterile ZK60-HA composites in Hank's solution after 1 h of immersion are plotted in Figure 49 and 50, respectively and the corresponding electrochemical parameters are listed in Table 13 and 14 respectively. Figure 51 shows the direct comparison between autoclaved and non autoclaved specimens tested in Hank's solution for a given composite, which shows that the autoclaved specimens have a slightly better corrosion resistance than non autoclaved samples. The autoclaved specimens have a nobler potential compared to the non autoclaved samples. Additionally, the autoclaved specimens show a passive range with a defined pitting potential.

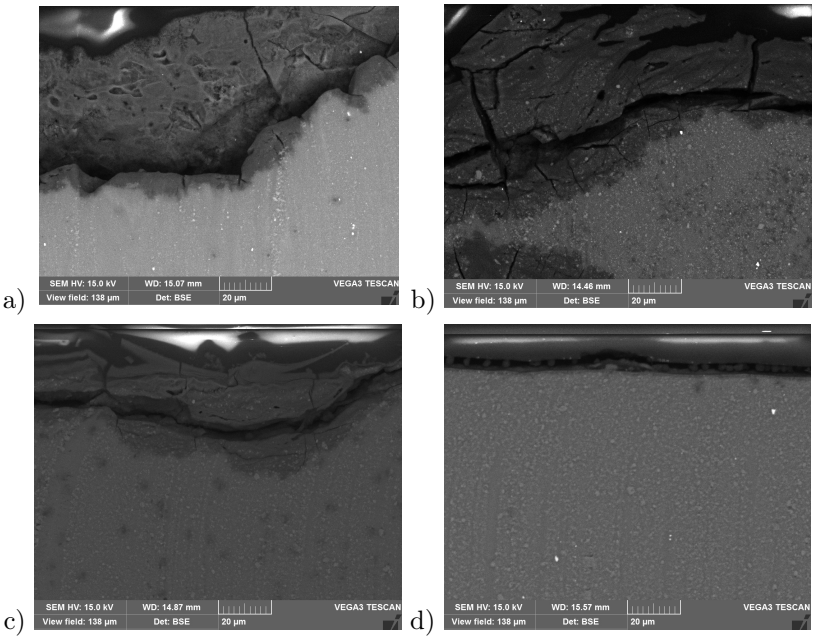

Figure 46 – *Cross section of composites after immersion, showing the outside layer of corrosion products, (a) ZK60, (b) ZK60-7.5, (c) ZK60-10 and (d) ZK60-20.*

Table 13 – Electrochemical parameters derived from potentiodynamic polarization curves in sterile specimens after 1 h of immersion in Hank's solution.

Material	E_{corr} (mV)	i_{corr} (μA/cm^2)	E_{pitt}-E_{corr} (mV)
ZK60	-1405.50	0.0035	81.90
ZK60-7.5	-1455.90	0.0062	98.00
ZK60-10	-1437.40	0.0036	112.50
ZK60-20	-1399.10	0.0017	92.60

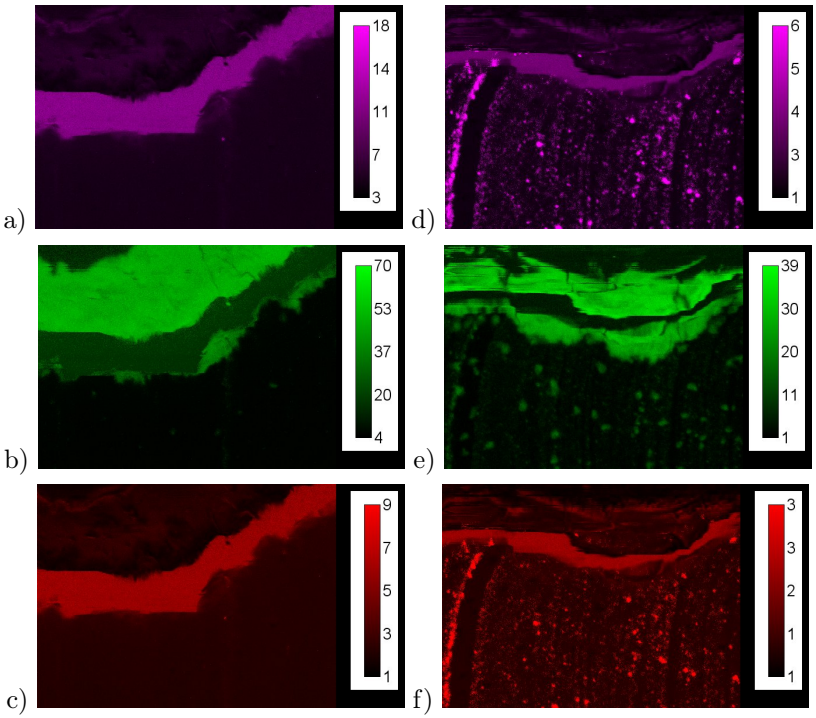

Figure 47 – *EDXS in the cross section of composites ZK60 showing the elements Ca (a), O (b) and P (c) and ZK60-10 showing the same constituents (d, e, f) respectively.*

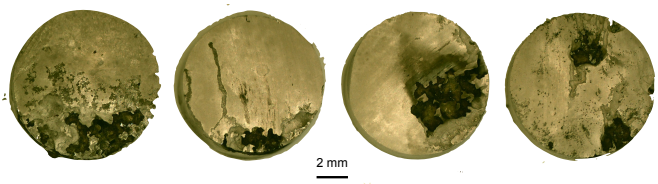

Figure 48 – *Specimens after immersion and corrosion products removal, showing the corrosion sites. From left to right, ZK60, ZK60-7.5, ZK60-10, ZK60-20.*

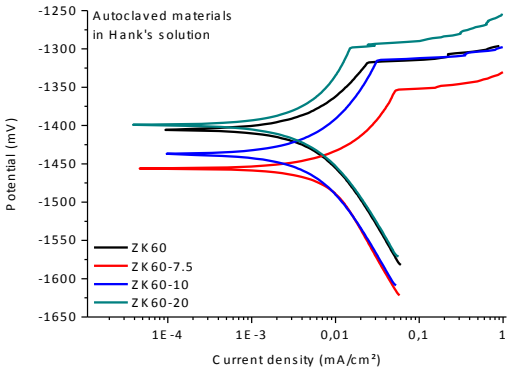

Figure 49 – *Potentiodynamic polarization curves of sterilized materials after 1 h of immersion in Hank's solution for all materials.*

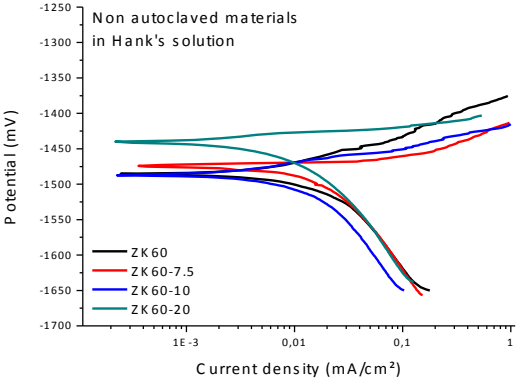

Figure 50 – *Potentiodynamic polarization curves of non sterilized materials after 1 h of immersion in Hank's solution for all materials.*

5.5.3.2 Effect of organic additives

Potentiodynamic polarization curves of autoclaved specimens in DMEM + 10 vol.% FBS solution are shown in Figure 52 and the derived parameters are in Table 15 showing the differences in potentials, current densities and pitting potential in the case of autoclaved specimens. It is

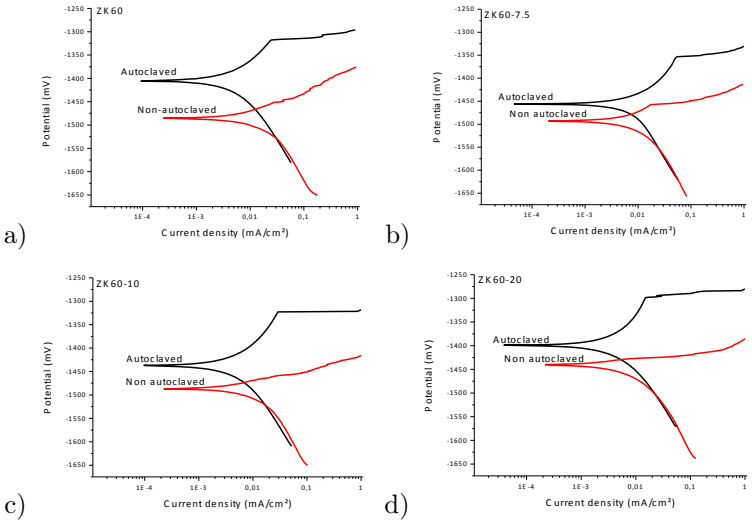

Figure 51 – *Potentiodynamic polarization curves showing the comparison between sterile and non sterile specimens by autoclaving after 1 h of immersion in Hank's solution. ZK60 (a), ZK60-7.5 (b), ZK60-10 (c), ZK60-20 (d).*

possible to observe that DMEM is a severe environment, which induced a lower corrosion resistance of the samples.

A comparison between sterile specimens corroded in DMEM + 10 vol.% FBS and in Hank's solution evidences their behaviour under the two different solutions, Figure 53. As in the comparison between sterile and non sterile specimens, there is also a difference in the corrosion resistance induced by the used solution. In this case, in Hank's solution was less corrosive and the material had a lower overall corrosion rate, compared to those assays in DMEM + 10 vol.% FBS.

Table 14 – Electrochemical parameters derived from potentiodynamic polarization curves in non sterile specimens after 1 h of immersion in Hank's solution.

Material	E_{corr} (mV)	i_{corr} (μA/cm^2)	E_{pitt}-E_{corr} (mV)
ZK60	-1485.40	0.0153	–
ZK60-7.5	-1458.30	0.0122	–
ZK60-10	-1487.10	0.0098	–
ZK60-20	-1440.40	0.0058	–

Table 15 – Electrochemical parameters derived from potentiodynamic polarization curves in sterile specimens after 1 h of immersion in DMEM + 10 vol.% FBS solution.

Material	E_{corr} (mV)	i_{corr} (μA/cm^2)	E_{pitt}-E_{corr} (mV)
ZK60	-1506.50	0.0847	–
ZK60-7.5	-1470.40	0.0453	–
ZK60-10	-1469.20	0.0643	–
ZK60-20	-1486.50	0.0453	–

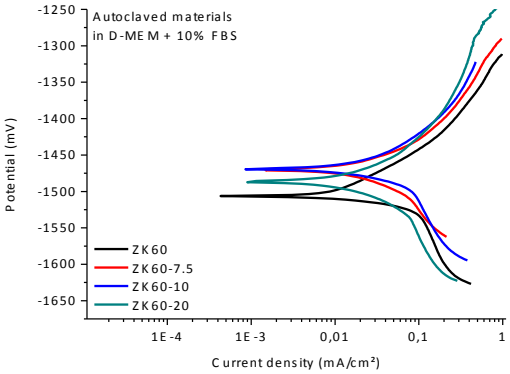

Figure 52 – *Potentiodynamic polarization curves of sterilized materials after 1 h of immersion in DMEM + 10 vol.% FBS solution for all materials.*

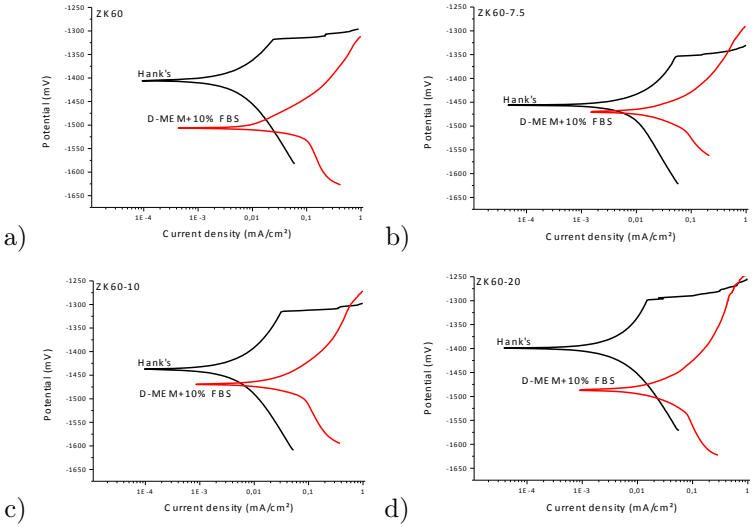

Figure 53 – *Potentiodynamic polarization showing the differences on tests after 1 h of immersion in Hank's and DMEM + 10 vol.% FBS solutions. ZK60 (a), ZK60-7.5 (b), ZK60-10 (c), ZK60-20 (d).*

6 DISCUSSION

6.1 BALL MILLING

After ball milling, it was observed that the higher the time length (up to 90 h) a better particle distribution was achieved. Time was then continuously reduced with the purpose of achieving a feasible production time, but keeping an acceptable HA distribution. The results show a long time experiment (20 h - sample 3), which is compared to other ball milling parameters (varying bpr and time) where the time length is feasible for material production. The microstructure of sample number 5 (milled for 7 h, with a bpr of 20:1 at 250 rpm), has a comparable HA distribution to that one milled for 20 h. That is mainly due to bpr, which is the major influent in this case, once more energy is involved in the process. This energy comes from an increase in the quantity of impacts per time unit, where a higher ratio of HA particles are being involved and well distributed in the ductile Mg matrix. If the bpr is low, either the speed or the time should be higher to compensate this energy loss, i.e., the material should be milled for either more time or at a higher ratio of grinding media impacts (crucible speed). Higher speeds cannot be used, due to temperature increase at these time lengths. As for time, it does not have to be as long when the ball-to-powder ratio is enough for achieving the desired microstructure. (STÜPP, 2013) Previous studies (WITTE et al., 2007; FENG; HAN, 2010, 2011) with other processing routes for producing composites did not achieve a very good particle distribution, where clustering was observed. This shows the importance of the powder preparation, where the reinforcement might be not well distributed when the two phases are not properly mixed, influencing the final mechanical properties and corrosion resistance of the composites.

After decreasing time from up to 90 h, the parameters *5*, *6* and *7* were chosen, which after analyzing (the acceptable particle distribution with feasible time lengths), parameters studied in sample 5 were therefore chosen for material production before extrusion (ball milling) due to microstructure features, mainly particle distribution.

With the SEM micrographs (Figure 34), hydroxyapatite is visible as the white constituent in the matrix. Also in Figure 34, EDXS shows the regions rich in Ca, evidencing the HA sites, since Ca is the major constituent of HA. Its distribution within the matrix is then seen, confirming what was presented with light microscopy. Further-

more, it supports the choice of the ball milling parameters to produce the powder for consolidating the composites with hot extrusion, sample 5 (milled for 7 h, with a bpr of 20:1 at 250 rpm).

6.2 EXTRUDED ALLOYS

For composites with higher ratio of hydroxyapatite (10% and 20%), temperature after extrusion was extremely high, up to 650°C. In these cases, the material either burned or experienced hot cracks on the surface. This happens due to high rate of material friction with the extruder wall, which is increased by HA addition. Also because HA isolates the heat and retards heat transfer, increasing material's temperature. Depending on the undergone friction and initial temperature, the material could easily exceed its eutectic temperature, cases in which burning was observed.

Up to the end of the heating chamber's path, the extrusion was indirect. After that, a small portion of the material was extruded directly. That caused the material in the middle to flow faster due to friction of the material in contact with the wall, which was migrating to the middle of the extruded cylinder, contaminating it. The portion where that happens is called secondary deformation zone.

6.3 MICROSTRUCTURE

HA is seen in the micrographs as black points. The micrograph of the ZK60 alloy without HA addition also shows black points in the matrix. That happens due to oxide dispersion which are developed from the oxide layer that formed in the surface of the Mg chips before ball milling. Some oxides are also developed during the material production (ball milling and hot extrusion).

With etching, it is possible to analyze the grain size and HA distribution in the microstructures of the alloy and its composites. There is a duplex distribution of the grain sizes with the microstructure mainly composed of fine grains with few regions containing coarse grains. These coarse grained regions align along the extrusion direction. With the addition of HA, the number of regions with coarse grains decrease and the fine grain regions become more prevalent, especially in the ZK60-20. In ZK60, ZK60-7.5 and ZK60-10, the coarse grain size ranges from 15 to 40 μm, while in ZK60-20, the coarse grained region

has a grain size less than 20 μm. The fine-grained regions contained grains that are less than 1 μm for all the materials. HA is homogeneously distributed throughout the samples resulting in the formation of fine grains, even though there is some agglomeration when the quantity of HA is increased. In ZK60 alloy the fine grained regions are due to the presence of oxide particles introduced during machining and ball milling.

ZK60 is a typical Mg-Zn-Zr alloy (ZENG et al., 2011). Zr also aids grain refinement of the microstructure and therefore is beneficial to the corrosion resistance of Mg alloys (SONG, 2005; ZENG et al., 2011). As expected, particle distribution is well improved by hot extrusion, since the addition of particles refines the grains of matrix during hot deformation and consequently, particle aggregation is almost eliminated by hot extrusion (WANG et al., 2012). HA was finely dispersed in the matrix, which is one of the most important features after extrusion. Due to these features, grain refining was also observed, similar to (WANG et al., 2012). The reduction in grain size with the addition of second phase particles was already stated by other works, Chen et al. (CHEN et al., 2010) shows that a substantial grain refining of a Mg matrix (AZ91D) occurs when ceramic particles (SiC) are added in a casting process.

Dynamic recrystallization (DRX) is one of the reasons for grain refinement. The addition of second phase particles as HA affect the DRX during hot deformation and also hinder the grain boundaries movement (grain growth), aiding grain refinement. It is also visible that there is a difference between grain sizes in particle rich zones, and areas where HA is not predominant. That indicates the influence of the particles on the DRX of the matrix. During deformation, this phenomenon is explained by the mismatch between a hard ceramic particle (non-deforming) and the ductile matrix, effect that can alter the local slip activity in the surroundings. This leads to a strain gradient near the particle, region which contains higher dislocation density and orientation gradient, aiding DRX and refining grains in the surroundings. (DOHERTY et al., 1997; WANG et al., 2012)

After extrusion, the present phases were determined by XRD. The XRD confirmed the dispersion of HA in the matrix with HA peaks, even though it is very poorly detected. That is due to low volume fraction of particles and because the hydroxyapatite is finely distributed in the magnesium matrix. Also, an intermetallic composed by Mg and Zn ($MgZn_2$) is formed after ball milling and hot extrusion. Magnesium oxide is also present, however it was not detected by the XRD, only after corrosion tests.

The composites' densities were theoretically calculated, measured and except for ZK60, they were very similar. The alloy without HA addition had a porosity of 0.01%, which is very small. This means the ball milling had the HA particles well distributed in the matrix and that the hot extrusion had the material well consolidated. During ball milling, the hard ceramic particles are pushed into the ductile ZK60 matrix, providing a very good interface. This interface Mg-HA is very important for all the composites' properties and so is the absence of pores. From all that, it is confirmed that ball milling plays the most important role in HA dispersion within the Mg matrix, which is improved by hot extrusion.

6.4 MECHANICAL PROPERTIES

Little amount volume fraction of ceramic particulates with smaller sizes has a significant influence on microstructure and consequently, in mechanical properties of particulate reinforced magnesium matrix composites (DENG et al., 2010). Mechanical properties of composites are improved by uniform particle distribution. Furthermore, the particle alignment might also improve the mechanical properties along the better particle distribution direction (extrusion direction), what is clearly shown with the hardness results. (WANG et al., 2012)

The tensile stress-strain curves show that up to 10 wt.% HA addition, the Yield strength has increased along with the ultimate tensile strength in detriment of the elongation, which was reduced to nearly 0%. When 20 wt.% HA was added, a decrease in the UTS was seen due to the brittle behaviour the great amount of HA induces in the material, through HA clustering and the hampering of dislocation movement, which hindered the basal plane slip, preventing plastic deformation of the ZK60 matrix. For that reason, there is no tensile yield strength (TYS) value in the Table. This means that when adding 20 wt.% HA, brittle behaviour is observed, and the material can come to rupture without increase of the applied strength, which is dangerous in some applications. This is similar to Feng and Han in their both works (FENG; HAN, 2010, 2011), where it was stated that from a specific amount of CPP addition, micropores were formed and a drop in the mechanical behaviour was observed. A slight increase in the Young's modulus (E) for the composites is also observed, based in the visible difference in the curves' slope. That was expected, since the two materials share their modulus (mixture rule (CALLISTER; RETHWISCH, 2007)) and HA has

a much higher Young's modulus than Mg, causing an increase in E for the composites.

Deng et al. (DENG et al., 2010) also studied the tensile properties in a Mg based composite. With a very low amount of SiC addition, there is an increase in TYS, once the grain is refined and the quantity of second phase particles is not substantial to induce a brittle behaviour in the Mg matrix. When the amount of SiC is further increased, there is a slight change in the TYS, which starts decreasing due to difficulty of matrix deformation and microcracks that appear in the agglomerated regions during tensile tests (DENG et al., 2010). When the particles are not well distributed and clusters are observed, these sites behave as voids in the structure, decreasing substantially the material's resistance.

The compression stress-strain curves show that the yield strength and the ultimate compressive strengths increase with the addition of HA, while the elongation to failure decreased. The reasons are similar to those presented for tensile tests. The only behaviour difference between tensile and compression tests is the definite Yield strength. This is explained by the hampering of twinning formation and dislocation movement. Because their movement is hindered, twins and dislocations start to pile up when a force attempts to deform the material. When the stress reaches the compressive yield strength (CYS), twinning starts to be formed and dislocations move at once, causing the abrupt deformation with a small decrease in the applied strength - forming the visible YS in the diagram.

For the composites, the CYS is higher, since HA and finer grains hinder the deformation of the matrix up to a higher strength. When analyzing pure Mg with HA addition, Del Campo et al. (CAMPO et al., 2014) observed that the CYS was decreasing when adding the ceramic particles. He explains that the critical resolved shear stress (CRSS) for the basal slip system is lower than the other slip systems, but that they are blocked by most grains in the extrusion direction, due to texture. It is then affirmed that the addition of HA decreases the intensity of texture and that more grains have favorable orientations for basal slip movement. When the basal slip has a favorable orientation, the material also deforms by basal slip (which is the only active slip system in Mg), causing the decrease in the YS. This is true probably because there is a mismatch between the reinforcement particles and the matrix, where the load cannot be properly transfered from the HA to the magnesium matrix. When the particles are well attached to the matrix as in the present work, even though the basal planes are activated

and the material is supposed to easily deform plastically, the second phase particles (with a good interface) would hamper its movement and prevent deformation, increasing the CYS, as observed here.

Hardness has a great similarity with stress-strain diagrams and the resemblance is consistent, since higher hardness is observed when adding HA. The explanation for that is the same as described above for compression and tensile samples, because hardness shows the material's resistance to plastic deformation. For the alloy without HA addition, one can see that the hardness measured in the cross section sample is higher, feature that changes when HA is added, because the particle distribution is better in the extrusion direction. It means HA has an important role in the composites' hardness, including the direction of the incoming force. The reason for the material to be harder when the force is applied in the longitudinal direction is that the second phase particles are better distributed in that direction. In that case, the indentation embraces more and better distributed particles, and so is necessary a higher strength for matrix's deformation. There are some reasons for the hardness to increase in a magnesium reinforced ceramic composite, which are the obstacles to dislocation movement and the grain size reduction, both significant features for mechanical properties, and already enlightened in the former Sections (DENG et al., 2010; JEONG; KIM, 2014).

6.5 CORROSION STUDIES

The microstructure of the materials has an influence on the final corrosion behavior. In the particular case of Mg-Ca alloys, it has been reported by Jeong and Kim (JEONG; KIM, 2014) that the corrosion resistance enhanced after extrusion. One of the reasons is due to the high degree of grain refinement and basal texture strengthening during extrusion. There are other factors, as a continuous intermetallic phase formation in the grain boundaries of the Mg matrix, but this does not happen here. It was also reported by other authors that a finer microstructure (small grain sizes and more grain boundaries) cause the rate of corrosion to decrease compared with a coarse-grained microstructure (ZHANG; JI; WU, 2011; JEONG; KIM, 2014).

Comparing ZK60 with the composites, it is visible that the area fraction associated with the localized corrosion does not seem to change significantly with the addition of HA. The reasons behind the localized corrosion are not yet very clear. It is proposed to be due to the rupture

of the very thin oxide layer that forms during autoclaving or due to inhomogeneous nature of this layer. Potentiodynamic polarization tests give a better insight in the influence of the thin oxide layer formed during sterilization, which is one the possible reasons for localized corrosion in the samples immersed in DMEM + FBS. Even though the sterilization process influenced the corrosion rate, immersion tests showed that HA slightly improves the corrosion resistance in immersed specimens.

The pH of the surrounding solution changed differently for every composite. It increased due to the formation of H_2 gas from ions H^+. Furthermore, the hydroxyl groups from the dissociated water stays in the solution. From the Pourbaix diagram (Figure 5), one can see that higher pH stabilizes the Mg hydroxide, product that forms the corrosion layer and protects the underneath material. Higher pH is, therefore, a concern because it inhibits cell proliferation and tissue formation (SONG, 2005; YUN et al., 2009). The lower pH also confirms that the corrosion in the composites is gradually less severe than in ZK60. Lower pH means that less H_2 bubbles and hydroxyls were generated and these groups are formed due to water dissociation, which is triggered by the release of Mg^+ ions in the solution.

According to Feng and Han (FENG; HAN, 2011), a dense structure of $Mg(OH)_2$ is formed, which is stabilized by Ca, present in HA. Here, a similar corrosion product is formed (MgOH), confirmed by XRD and EDXS. In the latter, Figure 47, three different layers were observed, outer most observed is MgOH, followed by a Ca layer rich in P and then again another MgOH layer attached to the ZK60 matrix. Furthermore, Feng and Han (FENG; HAN, 2010) also state that Zn helps stabilizing the protective layer. The corrosion layers formed are not dense and have micropores, explaining why the substract corrosion is slowed, but not ceased. This layer is also present in the base alloy samples, because such elements as Ca, P and O are present in the solution.

From the above described, a gradually lower corrosion rate was expected with the addition of HA. That happens when more than 7.5 wt.% is added, quantitatively. Visually, the samples seemed to have approximately the same amount of corrosion, with great areas of localized corrosion, when the rest of the specimen seemed to be intact. The presence of Zn might also have an influence in the corrosion behaviour. Ha et al. (HA et al., 2013) observed that alloyed Zn accelerates hydrogen evolution, leading to higher corrosion loss. The corrosion products based in hydroxyls ($Mg(OH)_2$ and $Zn(OH)_2$) form a layer of precipitate on the surface of the material, but when immersed in chloride containing solutions, the corrosion actively occurs when the metal hydroxide

reacts with the Cl^- groups. That happens due to the formation of highly soluble $MgCl_2$ from $Mg(OH)_2$. Because $MgCl_2$ is water soluble, the reaction breaks the integrity of $Mg(OH)_2$ and pitting corrosion is formed when Cl^- ions get into inner part of the material, as grain boundaries. (YE et al., 2010; HA et al., 2013)

The observed results after corrosion products removal, Figure 48 and Table 12 are similar to the previous observations (FENG; HAN, 2011) on ZK60 alloy containing CPP and AZ91 with HA in artificial seawater (WITTE et al., 2007). However, this result is contrasted with the results for pure Mg where an increase in the corrosion rate was detected with the addition of HA (GU et al., 2010).

All the sterile specimens showed a passive range in Hank's solution with E_{pitt} at approximately -1350 to -1300 mV. This behaviour is related to the oxide layer on top of the alloy, which was formed during autoclaving and partially protects the underneath material. There are differences in these values, which do not follow a pattern. This issue is attributed to the heterogeneity of this layer, Figure 43.

The non sterile specimens did not show a passive range. For them, the anodic branch of the curve experienced an abrupt increase in the current density with a very small change in the potential, which means the specimens corroded freely. That is observed, since there is no protective layer and consequently no barrier for the substract corrosion. It was seen that the corrosion of non sterile composites slightly improved with the addition of HA. This feature was not observed for sterile composites, probably due to the heterogeneous nature of the corrosion layer formed during autoclaving.

In the direct comparison between autoclaved and non autoclaved composites, it is clear that the sterile materials have a better corrosion resistance (nobler potentials, lower current densities and a passive range), until the protective layer is broken. The autoclaving forms an outer layer, which protects the material. This protection cannot be quantitatively measured, once the layer is not homogeneous, from which we assume autoclaving is not the very best sterilization method, once it changes the corrosion nature of the material.

The potentiodynamic polarization measurements in DMEM did not show a passive range. That suggests that there is no visible protective effect from the autoclaved oxide layer when the specimens are exposed to DMEM solution. With HA addition, a slightly lower i_{corr} and nobler E_{corr} are reported. The differences in the results once again did not follow a trend with the addition of HA and this is probably due to the oxide layer from autoclaving.

Directly comparing the experiments in Hank's and DMEM solution, it is easy to observe what was stated above. The experiments in DMEM show a higher i_{corr} and a more negative E_{corr}, meaning DMEM leads to a lower corrosion resistance of the materials. Furthermore, the oxide layer formed during autoclaving, which was seen to have a protective behaviour in Hank's solution, does not protect the composites under DMEM, indicating that DMEM is a much harsher corrosion environment.

When the Mg-Zn alloy gets in contact with the corroding solution, E_{corr} decreases and then starts to rise again. This gradual rise is due to the formation of the passive film during immersion time, which was shown here by meanings of XRD and EDXS and also observed by Ha et al. (HA et al., 2013).

With the addition of HA, a slight reduction of the corrosion densities was observed. It means that HA has no negative influence in the corrosion behaviour of the composites as it has been reported for other types of reinforcement as SiC (TIWARI; BALASUBRAMANIAM; GUPTA, 2007; PARDO et al., 2009) and alumina (BAKKAR; NEUBERT, 2007). The addition of HA brought the E_{corr} to nobler potentials except for ZK60-10 (which did not change significantly comparing to ZK60) and the i_{corr} decreased. ZK60-20 presented the noblest E_{corr} and the lowest i_{corr}, which might be related to more protective corrosion products HA can help forming and stabilizing. It was already explained that HA aids grain refining and studies confirmed the grain size influences the corrosion behaviour. Zeng et al. (ZENG et al., 2011) proved through electrochemical polarization tests that smaller grains improve the corrosion resistance of the ZK60 alloy.

The different outcomes found in this work related to corrosion resistance might be due to several factors: i) The microstructure of the alloy: the HA distribution is not totally homogeneous which might affect the final results and ii) The sterilization method: The oxide layer developed during autoclaving reveals a partial protective character but at the same time shows some irregularities.

The corrosion morphology of an alloy is directly linked with the anisotropy of the material. The grain size, distribution of intermetallic compounds and, in this case, the HA distribution.

7 CONCLUSIONS

ZK60 magnesium composites with different amounts of hydroxyapatite were successfully fabricated by ball milling and hot extrusion. The grain size of the composite decreased substantially, with addition of HA providing sites for nucleation. With the addition of HA, an increase in the compressive yield strength and ultimate compressive strength was observed in the composites, while the compression to fracture decreased.

Regarding to corrosion behavior, immersion tests showed that the corrosion rate decreases with more than 10 wt.% HA, while it increases slightly with 7.5 wt.% HA. It was also shown that the corrosion is general corrosion with some localized corrosion likely to be due to the inhomogeneity of the autoclaved oxide layer. Potentiodynamic polarization curves in autoclaved specimens within Hank's solution showed the same trend, except that for ZK60-7.5, there is a small increase in current density compared to ZK60, and it only decreases when adding 20 wt.%. In DMEM + 10 vol.% FBS, the difference is clearer. By adding any amount of HA, corrosion density decreases in overall, and potentials are nobler, indicating an improvement in the corrosion resistance of the autoclaved composites developed.

A summary of the corrosion behaviour of the materials is:

- There is an effect of the sterilization method on the final corrosion behaviour. Specimens treated with autoclaving show a higher corrosion resistance that might be due to the formation of a partial protective oxide layer on the surface,
- The addition of HA does not show a negative influence in the corrosion properties and
- There is a decrease of the corrosion resistance of the materials in the presence of organic compounds.

REFERENCES

AGRAWAL, C. M. Reconstructing the human body using biomaterials. *JOM*, Springer, v. 50, n. 1, p. 31–35, 1998.

AL-SAMMAN, T. *Magnesium: The Role of Crystallographic Texture, Deformation Conditions and Alloying Elements on Formability*. Tese (Doutorado) — Cuvillier Verlag Göttingen, 2008.

AVEDESIAN, M. M.; BAKER, H. et al. *Magnesium and magnesium alloys*. [S.l.]: ASM international, 1999.

BAKKAR, A.; NEUBERT, V. Corrosion characterization of alumina-magnesium metal matrix composites. *Corrosion Science*, Elsevier, v. 49, n. 3, p. 1110–1130, 2007.

BETTLES, C.; GIBSON, M. Current wrought magnesium alloys: strengths and weaknesses. *JOM*, Springer, v. 57, n. 5, p. 46–49, 2005.

CALLISTER, W. D.; RETHWISCH, D. G. *Materials science and engineering: an introduction*. [S.l.]: Wiley New York, 2007.

CAMPO, R. del et al. Mechanical properties and corrosion behavior of Mg–HAP composites. *Journal of the Mechanical Behavior of Biomedical Materials*, Elsevier, v. 39, p. 238–246, 2014.

CHEN, T. J. et al. Grain refinement of AZ91D magnesium alloy by SiC. *Journal of Alloys and Compounds*, Elsevier, v. 496, n. 1, p. 218–225, 2010.

CZERWINSKI, F. et al. *Magnesium Alloys - Design, Processing and Properties*. [S.l.]: InTech: Rijeka, Croatia, 2011.

DENG, K. K. et al. Effect of particle size on microstructure and mechanical properties of SiCp/AZ91 magnesium matrix composite. *Materials Science and Engineering*, Elsevier, v. 543, p. 158–163, 2012.

DENG, K. K. et al. Effect of submicron size SiC particulates on microstructure and mechanical properties of AZ91 magnesium matrix composites. *Journal of Alloys and Compounds*, Elsevier, v. 504, n. 2, p. 542–547, 2010.

DOHERTY, R. D. et al. Current issues in recrystallization: a review. *Materials Science and Engineering: A*, Elsevier, v. 238, n. 2, p. 219–274, 1997.

EMLEY, E. F. *Principles of Magnesium Technology*. [S.l.]: Elsevier Science and Technology, 1996.

FENG, A.; HAN, Y. The microstructure, mechanical and corrosion properties of calcium polyphosphate reinforced ZK60A magnesium alloy composites. *Journal of Alloys and Compounds*, Elsevier, v. 504, n. 2, p. 585–593, 2010.

FENG, A.; HAN, Y. Mechanical and *in vitro* degradation behavior of ultrafine calcium polyphosphate reinforced magnesium-alloy composites. *Materials and Design*, Elsevier, v. 32, n. 5, p. 2813–2820, 2011.

FULMER, M. T. et al. Measurements of the solubilities and dissolution rates of several hydroxyapatites. *Biomaterials*, v. 23, n. 3, p. 751–755, 2002.

GU, X. et al. Microstructure, mechanical property, bio-corrosion and cytotoxicity evaluations of Mg/HA composites. *Materials Science and Engineering: C*, Elsevier, v. 30, n. 6, p. 827–832, 2010.

HA, H. Y. et al. Limitations in the use of the potentiodynamic polarisation curves to investigate the effect of Zn on the corrosion behaviour of as-extruded Mg–Zn binary alloy. *Corrosion Science*, Elsevier, v. 75, p. 426–433, 2013.

HASSAN, S. F.; GUPTA, M. Effect of type of primary processing on the microstructure, CTE and mechanical properties of magnesium/alumina nanocomposites. *Composite structures*, Elsevier, v. 72, n. 1, p. 19–26, 2006.

HAYDEN, H. W.; MOFFATT, W. G.; WULFF, J. *The structure and properties of materials, Volume 3: mechanical behavior*. [S.l.]: John Wiley and Sons: New York, USA, 1965.

HE, S. Y. et al. Microstructure and properties of biodegradable Beta-TCP reinforced Mg-Zn-Zr composites. *Transactions of Nonferrous Metals Society of China*, v. 21, n. 4, p. 814–819, 2011.

HOWLETT, C. R. et al. The effect of magnesium ion implantation into alumina upon the adhesion of human bone derived cells. *Journal*

of Materials Science: Materials in Medicine, Springer, v. 5, n. 9-10, p. 715–722, 1994.

JEONG, Y. S.; KIM, W. J. Enhancement of mechanical properties and corrosion resistance of Mg–Ca alloys through microstructural refinement by indirect extrusion. *Corrosion Science*, Elsevier, v. 82, p. 392–403, 2014.

JOCHEMS, C. E. et al. The use of fetal bovine serum: ethical or scientific problem? *Atla-Nottingham*, Fund for Replacement of Animals in Medical Experiments; 1999, v. 30, n. 2, p. 219–228, 2002.

KAINER, K. U. *Magnesium - Alloys and Technology*. [S.l.]: Wiley-VCH: Weinheim, Germany, 2003.

KAMMER, C. *Magnesium Taschenbuch*. [S.l.]: Aluminium Verlag: Düsseldorf, Germany, 1998.

KIRKLAND, N. T.; BIRBILIS, N. *Magnesium Biomaterials: Design, Testing, and Best Practice*. [S.l.]: Springer, 2013.

KLEIN, C. P. A. T. et al. Studies of the solubility of different calcium phosphate ceramic particles *in vitro*. *Biomaterials*, Elsevier, v. 11, n. 7, p. 509–512, 1990.

KUHLMANN, J. et al. Fast escape of hydrogen from gas cavities around corroding magnesium implants. *Acta Biomaterialia*, Elsevier, v. 9, n. 10, p. 8714–8721, 2013.

LI, J. Y. et al. Microstructural evolution of AZ91 magnesium alloy during extrusion and heat treatment. *Transactions of Nonferrous Metals Society of China*, Elsevier, v. 22, n. 5, p. 1028–1034, 2012.

LI, Z. *Mg/Hydroxyapatite composites for potential bio-medical applications*. Tese (Doutorado) — Brunel University, London, 2010.

LIN, X. et al. The *in vitro* degradation process and biocompatibility of a ZK60 magnesium alloy with a forsterite-containing micro-arc oxidation coating. *Acta Biomaterialia*, Elsevier, v. 9, n. 10, p. 8631–8642, 2013.

LIU, J. et al. Synthesis of Mg-Alumina nanocomposites by mechanical alloying. *Journal of Alloys and Compounds*, Elsevier, v. 563, p. 165–170, 2013.

LIU, M. et al. The influence of yttrium (Y) on the corrosion of Mg-Y binary alloys. *Corrosion Science*, Elsevier, v. 52, n. 11, p. 3687–3701, 2010.

MONMATURAPOJ, N. Nano-size hydroxyapatite powders preparation by wet-chemical precipitation route. *Journal of Metals, Materials and Minerals*, v. 18, n. 1, p. 15–20, 2008.

MUDALI, U. K.; SRIDHAR, T. M.; RAJ, B. Corrosion of bio-implants. *Sadhana Academy Proceedings in Engineering Sciences*, v. 28, n. 3-4, p. 601–637, 2003.

MYSHLYAEV, M. M. et al. Twinning, dynamic recovery and recrystallization in hot worked Mg-Al-Zn alloy. *Materials Science and Engineering*, Elsevier, v. 337, n. 1, p. 121–133, 2002.

NEWELL, J. *Essentials of modern materials science and engineering.* [S.l.]: Wiley Global Education: USA, 2009.

NG, W.; WONG, M.; CHENG, F. Stearic acid coating on magnesium for enhancing corrosion resistance in hanks' solution. *Surface and Coatings Technology*, v. 204, n. 11, p. 1823–1830, 2010.

NG, W. F.; CHIU, K. Y.; CHENG, F. T. Effect of pH on the *in vitro* corrosion rate of magnesium degradable implant material. *Materials Science and Engineering*, Elsevier, v. 30, n. 6, p. 898–903, 2010.

NIE, K. B. et al. Effect of hot extrusion on microstructures and mechanical properties of SiC nanoparticles reinforced magnesium matrix composite. *Journal of Alloys and Compounds*, Elsevier, v. 512, n. 1, p. 355–360, 2012.

PARDO, A. et al. Corrosion behaviour of silicon-carbide-particle reinforced AZ92 magnesium alloy. *Corrosion Science*, Elsevier, v. 51, n. 4, p. 841–849, 2009.

PARK, J. B.; BRONZINO, J. D. *Biomaterials: principles and applications.* [S.l.]: CRC Press: Boca Raton, USA, 2000.

PEKGULERYUZ, M. O.; KAINER, K. U.; KAYA, A. A. *Fundamentals of magnesium alloy metallurgy.* [S.l.]: Woodhead publishing limited: Cambridge, UK, 2013.

PRASAD, A. S.; OBERLEAS, D. Zinc: Human nutrition and metabolic effects. *Annals of Internal Medicine*, Am Coll Physicians, v. 73, n. 4, p. 631–636, 1970.

RAQUEZ, J. M. et al. Polylactide (PLA)-based nanocomposites. *Progress in Polymer Science*, Elsevier, v. 38, n. 10, p. 1504–1542, 2013.

SHEN, M. J. et al. Effect of bimodal size SiC particulates on microstructure and mechanical properties of AZ31B magnesium matrix composites. *Materials and Design*, Elsevier, v. 52, p. 1011–1017, 2013.

SONG, G. Recent progress in corrosion and protection of magnesium alloys. *Advanced Engineering Materials*, Wiley Online Library, v. 7, n. 7, p. 563–586, 2005.

SONG, G. Control of biodegradation of biocompatable magnesium alloys. *Corrosion Science*, n. 49, p. 1696–1701, 2007.

SONG, G.; ATRENS, A. Understanding magnesium corrosion. *Advanced Engineering Materials*, v. 5, n. 12, p. 837–858, 2003.

STAIGER, M. P. et al. Magnesium and its alloys as orthopedic biomaterials: a review. *Biomaterials*, Elsevier, v. 27, n. 9, p. 1728–1734, 2006.

STÜPP, C. A. Powder metallurgical synthesis of magnesium-apatite feedstock material. Diplomathesis: Developed and presented at Helmholtz-Zentrum Geesthacht - Germany, published at Santa Catarina's Federal University - Brazil. 2013.

SURYANARAYANA, C. Mechanical alloying and milling. *Progress in Materials Science*, Elsevier, v. 46, n. 1, p. 1–184, 2001.

TIWARI, S.; BALASUBRAMANIAM, R.; GUPTA, M. Corrosion behavior of SiC reinforced magnesium composites. *Corrosion Science*, Elsevier, v. 49, n. 2, p. 711–725, 2007.

UHTHOFF, H. K.; POITRAS, P.; BACKMAN, D. S. Internal plate fixation of fractures: short history and recent developments. *Journal of Orthopaedic Science*, Springer, v. 11, n. 2, p. 118–126, 2006.

VORMANN, J. Magnesium: nutrition and metabolism. *Molecular Aspects of Medicine*, n. 24, p. 27–37, 2003.

WANG, X. J. et al. Hot extrusion of SiCp/AZ91 Mg matrix composites. *Transactions of Nonferrous Metals Society of China*, n. 22, p. 1912–1917, 2012.

WANG, X. J. et al. Processing, microstructure and mechanical properties of micro-SiC particles reinforced magnesium matrix composites fabricated by stir casting assisted by ultrasonic treatment processing. *Materials and Design*, Elsevier, v. 57, p. 638–645, 2014.

WITTE, F. et al. Biodegradable magnesium-hydroxyapatite metal matrix composites. *Biomaterials*, v. 28, n. 13, p. 2163–2174, 2007.

WITTE, F. et al. *In vitro* and *in vivo* corrosion measurements of magnesium alloys. *Biomaterials*, v. 27, n. 7, p. 1013–1018, 2006.

WITTE, F. et al. Degradable biomaterials based on magnesium corrosion. *Current Opinion in Solid State and Materials Science*, v. 12, n. 5-6, p. 63–72, 2008.

WWW.FORTECH.ZCU.CZ. *Fortech Research Centre*. October 2014.

WWW.LIFETECHNOLOGIES.COM. *Life Technologies*. July 2014.

WWW.MATWEB.COM. *Matweb: material property data*. March 2014.

WWW.SUBSTECH.COM. *Extrusion*. June 2014.

WWW.TUCHEMNITZ.DE. *Technische Universität Chemnitz*. June 2014.

YAMAGUCHI, M. Role of zinc in bone formation and bone resorption. *The Journal of Trace Elements in Experimental Medicine*, Wiley Online Library, v. 11, n. 2-3, p. 119–135, 1998.

YE, X. et al. In vitro corrosion resistance and cytocompatibility of nano-hydroxyapatite reinforced Mg–Zn–Zr composites. *Journal of Materials Science: Materials in Medicine*, Springer, v. 21, n. 4, p. 1321–1328, 2010.

YUN, Y. et al. Revolutionizing biodegradable metals. *Materials Today*, Elsevier, v. 12, n. 10, p. 22–32, 2009.

ZENG, R. et al. Corrosion of an extruded magnesium alloy ZK60 component - the role of microstructural features. *Journal of Alloys and Compounds*, Elsevier, v. 509, n. 13, p. 4462–4469, 2011.

ZHANG, T.; JI, Z.; WU, S. Effect of extrusion ratio on mechanical and corrosion properties of AZ31B alloys prepared by a solid recycling process. *Materials & Design*, Elsevier, v. 32, n. 5, p. 2742–2748, 2011.

ZHANG, X. et al. Microstructure, mechanical properties, biocorrosion behavior, and cytotoxicity of as-extruded Mg-Nd-Zn-Zr alloy with different extrusion ratios. *Journal of Mechanical Behavior of Biomedical Materials*, n. 9, p. 153–162, 2012.

ZHAO, M. C. et al. Influence of homogenization annealing of AZ91 on mechanical properties and corrosion behavior. *Advanced Engineering Materials*, Wiley Online Library, v. 10, n. 1-2, p. 93–103, 2008.

ZHENG, Y. F.; GU, X. N.; WITTE, F. Biodegradable metals. *Materials Science and Engineering: R: Reports*, Elsevier, v. 77, p. 1–34, 2014.